JOURNAL OF GEOPHYSICAL RESEARCH, VOL. 106, NO. B11, PAGES 26,561–26,591, NOVEMBER 10, 2001

# Fluvial incision and tectonic uplift across the Himalayas of central Nepal

J. Lavé[1] and J. P. Avouac

Laboratoire de Géophysique, Commisariat à l'Energie Atomique, Bruyères-Le-Châtel, France

**Abstract.** The pattern of fluvial incision across the Himalayas of central Nepal is estimated from the distribution of Holocene and Pleistocene terraces and from the geometry of modern channels along major rivers draining across the range. The terraces provide good constraints on incision rates across the Himalayan frontal folds (Sub-Himalaya or Siwaliks Hills) where rivers are forced to cut down into rising anticlines and have abandoned numerous strath terraces. Farther north and upstream, in the Lesser Himalaya, prominent fill terraces were deposited, probably during the late Pleistocene, and were subsequently incised. The amount of bedrock incision beneath the fill deposits is generally small, suggesting a slow rate of fluvial incision in the Lesser Himalaya. The terrace record is lost in the high range where the rivers are cutting steep gorges. To complement the terrace study, fluvial incision was also estimated from the modern channel geometries using an estimate of the shear stress exerted by the flowing water at the bottom of the channel as a proxy for river incision rate. This approach allows quantification of the effect of variations in channel slope, width, and discharge on the incision rate of a river; the determination of incision rates requires an additional lithological calibration. The two approaches are shown to yield consistent results when applied to the same reach or if incision profiles along nearby parallel reaches are compared. In the Sub-Himalaya, river incision is rapid, with values up to 10-15 mm/yr. It does not exceed a few millimeters per year in the Lesser Himalaya, and rises abruptly at the front of the high range to reach values of ~4-8 mm/yr within a 50-km-wide zone that coincides with the position of the highest Himalayan peaks. Sediment yield derived from the measurement of suspended load in Himalayan rivers suggests that fluvial incision drives hillslope denudation of the landscape at the scale of the whole range. The observed pattern of erosion is found to closely mimic uplift as predicted by a mechanical model taking into account erosion and slip along the flat-ramp-flat geometry of the Main Himalayan Thrust fault. The morphology of the range reflects a dynamic equilibrium between present-day tectonics and surface processes. The sharp relief together with the high uplift rates in the Higher Himalaya reflects thrusting over the midcrustal ramp rather than the isostatic response to reincision of the Tibetan Plateau driven by late Cenozoic climate change, or late Miocene reactivation of the Main Central Thrust.

## 1. Introduction

The kinematics of mountain building results from the combination of crustal deformation and erosion, with the two processes being possibly coupled [e.g., *Koons*, 1989; *Molnar and England*, 1990; *Willet et al.*, 1993; *Avouac and Burov*, 1996]. This coupling arises because denudation depends on topography, while erosion influences tectonic processes by controlling boundary conditions at the Earth's surface through deposition and denudation. Another reason for this coupling is that erosion depends on climate, which is itself submitted to orographic forcing [e.g., *Masek et al.*, 1994]. As a result, tectonic uplift and denudation generally tend to balance each other, so that high denudation rates are found to correlate with zones of active mountain building [*Anhert*, 1970; *Pinet and Souriau*, 1988; *Summerfield and Hulton*, 1994; *Hovius*, 2000]. Mountain building thus leads to a complex loop with various feedback mechanisms linking crustal deformation, denudation, and climate. The Himalayas are often cited as the modern archetype where this kind of coupling may be at work. For example, headward erosion along the rivers cutting the edge of the Tibetan Plateau would have induced uplift of the Himalayan peaks through isostatic rebound, enhancing orographic precipitation and hence denudation [*Molnar and England*, 1990; *Burbank*, 1992; *Masek et al.*, 1994; *Montgomery*, 1994]. Such a process would explain the position of the front of the high range paradoxically well to the north of the main active thrust faults, i.e., the frontal thrusts. It would also drive accelerated uplift, independent of the kinematics of active thrust faulting, in response to climate change during the Cenozoic [*Molnar and England*, 1990; *Burbank*, 1992]. The building of the Himalayas would, moreover, have affected global climate by modifying the chemistry of the ocean and atmosphere [e.g., *Raymo et al.*, 1988; *Raymo and Ruddiman*, 1992]. This latter effect depends on the nature of the rocks that are uplifted, eroded, and

[1]Now at Laboratoire de Géodynamique des Chaînes Alpines, Grenoble, France.



Paper number 2001JB000359.
0148-0227/01/2001JB000359$09.00

weathered [e.g., *Derry and France Lanord*, 1997]. A better understanding of the kinematics of crustal deformation and the pattern of erosion in the Himalayas might therefore provide basic insight into mountain building processes. It would also help assess the eventual effect of the Himalayan orogeny on weathering fluxes and the effect of Cenozoic climate change on uplift.

In this paper, we document the pattern of denudation in the Himalayas of central Nepal by analyzing fluvial incision along some of the major rivers draining across the range (Figure 1). We first review the geological and geomorphological setting of the study area that encompasses most the Himalayas of Nepal (Figures 1 and 2). We then present the result of our survey of abandoned terraces. This study complements earlier investigations of abandoned fluvial terraces in the Siwalik Hills [*Nakata*, 1972; *Delcaillau*, 1992; *Lavé and Avouac*, 2000] and in the Lesser Himalaya [*Iwata et al.*, 1982; *Yamanaka and Iwata*, 1982; *Fort*, 1993]. In the high range the rivers generally flow along steep N-S gorges where terraces could not be preserved or may even never have formed, with stream gradients systematically steeper by a factor 10 compared to those along their upper and lower reaches. *Seeber and Gornitz* [1983] previously noticed this systematic steepening which they interpreted as an indicator of rapid river incision. In the absence of a terrace record we follow their line of thought and attempt to determine fluvial incision from the geometry of the modern channels. Using the tie points provided by the terrace survey in the Sub-Himalaya and Lesser Himalaya, we determine and calibrate a simple empirical relationship based on the estimated fluvial shear stress exerted by the flowing water on the streambed, and we use it as a proxy for fluvial incision along mountain rivers. We apply the method to all the major rivers draining the central Himalayas. We compare fluvial incision with mean denudation rates as estimated from measured suspended load at gauging stations along the studied rivers in order to test whether the landscape is eroded at the same rate as river downcutting. In section 6 we expand on tectonic implications in order to discriminate between different models of Cenozoic uplift and landscape evolution and discuss the significance of the present morphology of the range.

## 2. Overview of Himalayan Tectonics and Topography

### 2.1. Geomorphological and Geological Setting

Different geographic domains can be distinguished across the Himalayas of Nepal (Figures 1 and 2). The Siwaliks Hills form the most frontal relief just north of the Indo-Gangetic Plain. They are composed of easily erodible Neogene molasse accumulated in the foreland and deformed by thin-skinned tectonics (Figure 2). They form rows of hills with elevations below 1000 m (Figure 1b), separated by narrow elongated piggyback basins (called Dun in Nepali). Just north of this Sub-Himalayan fold belt, the higher relief of Mahabarat range is much more impressive reaching elevations up to 2500-3000 m (Figure 1b). The range consists mainly of schist and gneiss intruded by Late Cambrian to Ordovician granites and overlain by Cambrian to Eocene "Thetysian" sediments. These units belong to a crystalline sheet overlying the Lesser Himalaya (LH). The rocks in the LH consist of low-grade metasediments (phyllite, quartzite, and limestone of Devonian or older ages) forming a large antiformal duplex structure (Figure 2) [e.g., *Schelling*, 1992]. North of a line trending about N108°E (white dashed line on Figure 1b), the topography rises abruptly from elevations around 500-1000 m to more than 6000 m. This break in slope marks the front of the Higher Himalaya (HH). The highest Himalayan peaks lie only ~30-60 km north of this line (Figures 1b and 2). The crystalline units of the HH consist mainly of medium- to high-grade gneiss with large leucogranitic plutons of Miocene age [e.g., *Le Fort*, 1986; *Searle*, 1999]. The Tibetan Plateau, with its Thetysian sedimentary cover, extends to the north at elevations around 5000 m (Figure 2).

The boundaries between the different domains roughly coincide with major thrust faults. The Main Central Thrust (MCT) is a ductile shear zone that separates the LH from the HH [e.g., *Le Fort*, 1986]. The Main Boundary Thrust (MBT) marks the limit between the Sub-Himalaya and the LH, and the Main Frontal Thrust (MFT) bounds the southern limit of the Sub-Himalaya, at the front of the Siwalik Hills. All these thrust faults may connect to a single detachment at depth, that may be called Main Himalayan Thrust (MHT), as suggested

**Figure 1.** (opposite) (a) Geological and (b) geomorphological setting of study area. Geology from Nepalese 1:50,000 geological map (courtesy of the Department of Mines and Geology of Nepal), *Schelling* [1992], *Brunel* [1986], and *Stöcklin* [1980] and, for the Tibetan part, from *Gansser* [1964]. Faults were reported from *Yeats and Lillie* [1991]. MBT, Main Boundary Thrust; MCT, Main central Thrust; MFT, Main Frontal Thrust. Thick black lines follow the six trans-Himalayan rivers for which fluvial shear stress is calculated in this study. Down valley extent (white arcuate segment) of area shaped prominently by glacial erosion [*Duncan et al.*, 1998] define the beginning of dominant valley shaping by fluvial incision and domains of validity of our fluvial incision model. The white oval dots show locations where dated Holocene terraces could be used to calibrate rates of fluvial incision for this model. The N108°E white dashed line in Figure 1b follows the break in slope in front of the high range where intense microseismicity tends to cluster (microseismicity recorded between 1994 and 1998, courtesy of the Seismological laboratory, Department of Mines and Geology). This break in slope lies 30 to 60 km south of the highest Himalayan peaks (white triangles). From west to east >8000 m high summits are labeled by letters: D, Dhaulagiri; A, Annapurna; M,Manaslu; X, Shisha Pangma; C, Cho Oyu; E, Everest; L, Lhotse; M, Makalu; K, Kanchengjunga.

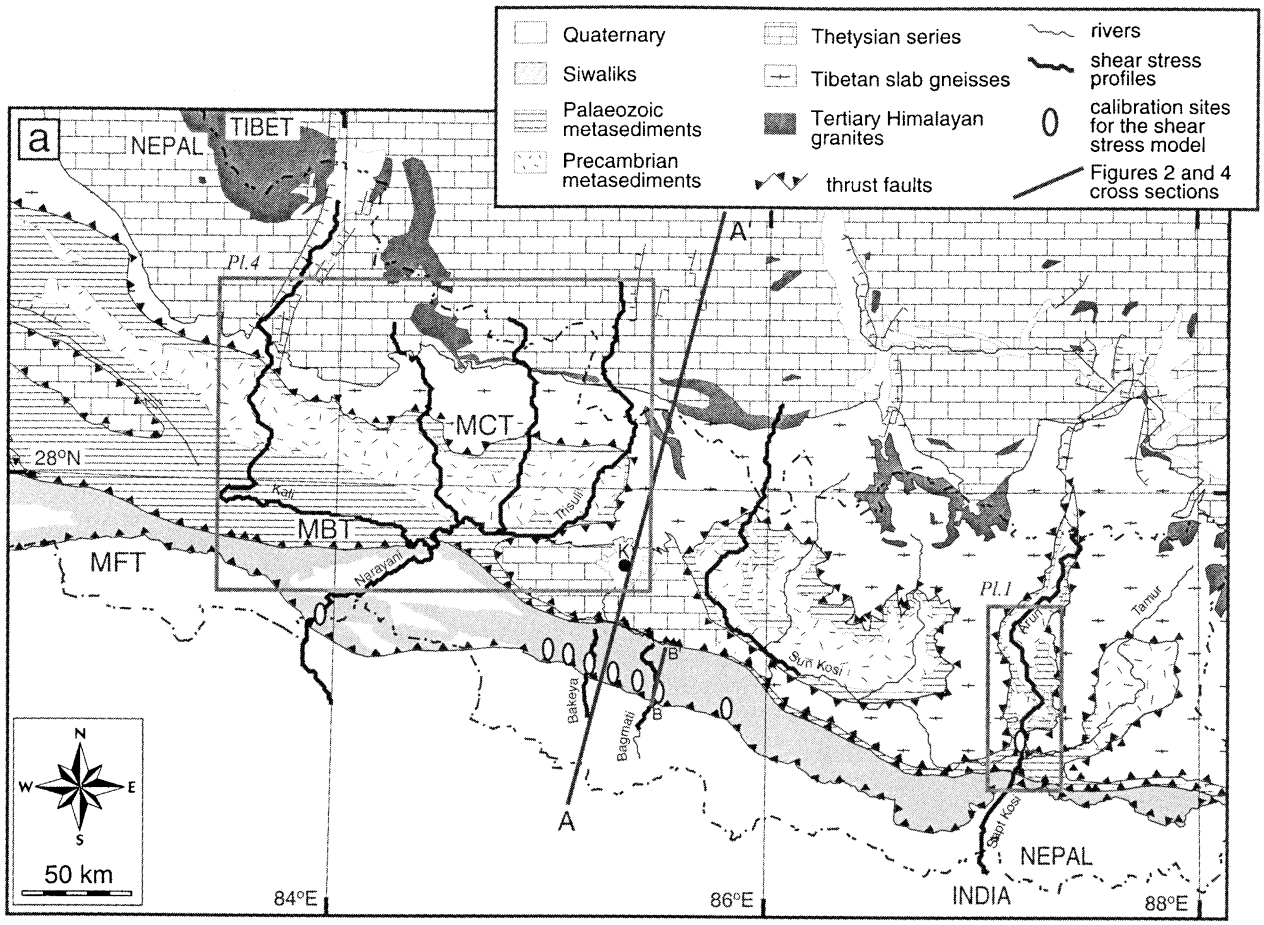
a
Quaternary
Siwaliks
Palaeozoic metasediments
Precambrian metasediments
Thetysian series
Tibetan slab gneisses
Tertiary Himalayan granites
thrust faults
rivers
shear stress profiles
calibration sites for the shear stress model
Figures 2 and 4 cross sections
NEPAL
TIBET
Pl.4
Pl.1
MCT
MBT
MFT
28°N
Kali
Trisuli
Narayani
Bakeya
Bagmati
Sun Kosi
Arun
Tamur
Sapt Kosi
A
A'
B
B'
K
N
W
E
S
50 km
84°E
86°E
88°E
INDIA
NEPAL

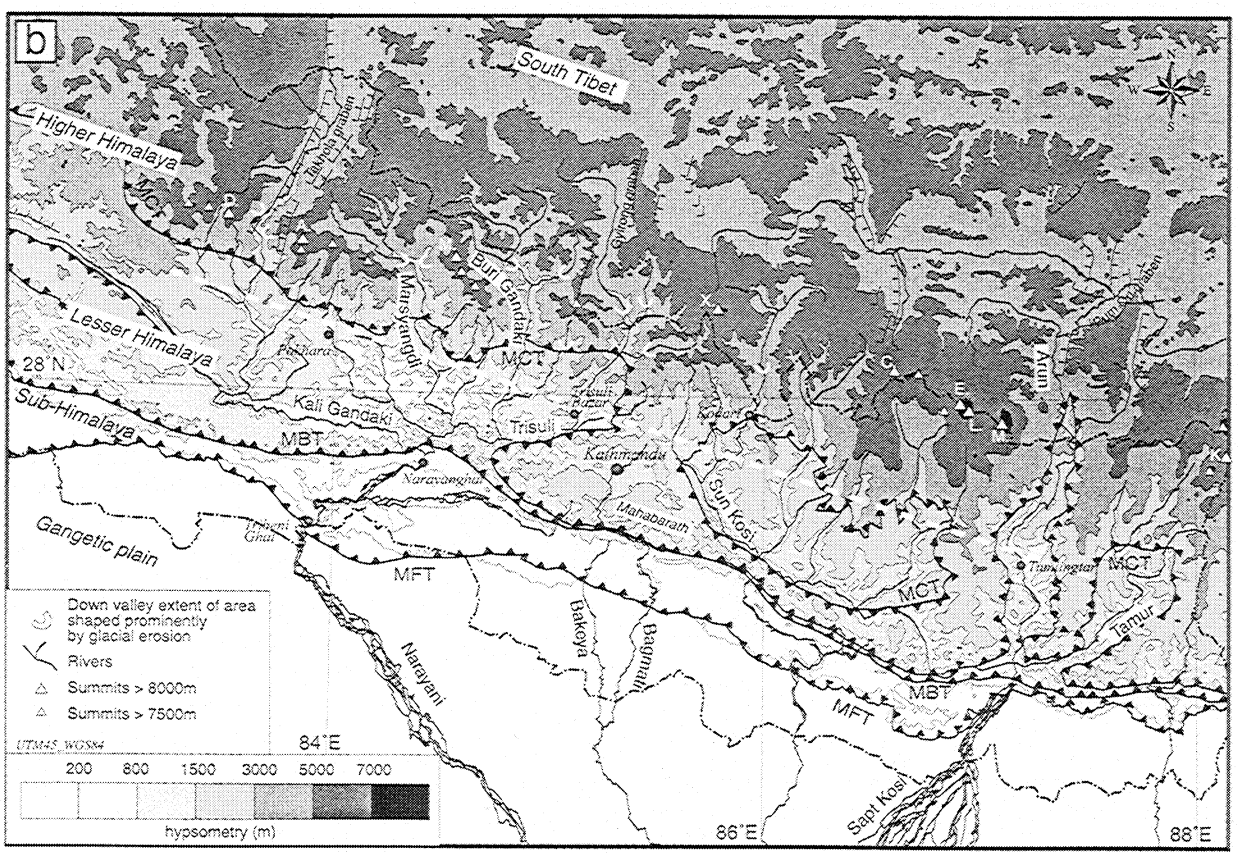
b
South Tibet
Higher Himalaya
Lesser Himalaya
Sub-Himalaya
Gangetic plain
MCT
MBT
MFT
28°N
Pokhara
Kali Gandaki
Trisuli
Kathmandu
Narayanghat
Mahabarath
Sun Kosi
Bakeya
Bagmati
Narayani
Arun
Tamur
Sapt Kosi
Down valley extent of area shaped prominently by glacial erosion
Rivers
Summits > 8000m
Summits > 7500m
UTM45_WGS84
84°E
86°E
88°E
200
800
1500
3000
5000
7000
hypsometry (m)

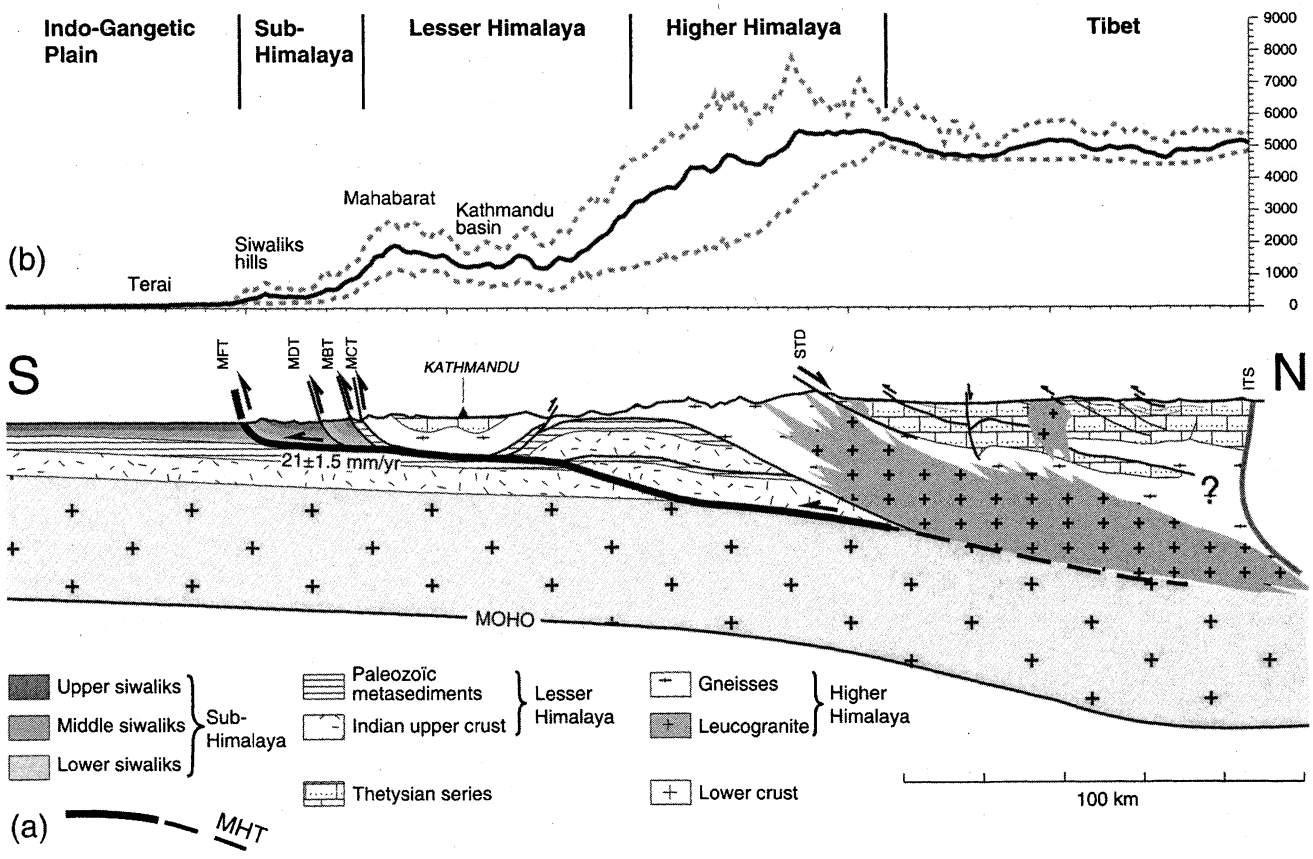


**Figure 2.** N18°E (a) geological section and (b) topography across the Himalayas at the longitude of Kathmandu modified from *Brunel* [1986]. Following *Schelling* [1992], the duplex structure in the Lesser Himalaya was derived from the antiform defined by foliation planes. The geometry of the Main Himalayan Thrust (MHT) was derived from this assumption and from balancing various sections in the Sub-Himalaya [*Schelling and Arita*, 1991; *Lavé and Avouac*, 2000]. The ramp beneath the high range connects with a flat that roughly coincides with the midcrustal reflector observed by INDEPTH1 experiment, 300 km east of the section [*Zhao et al.*, 1993]. The inferred geometry of the Moho approximately follows the elastic deflection that matches gravity data at the longitude of Mount Everest [*Lyon-Caen and Molnar*, 1983]. The lines in the Figure 2a show average topography (solid line) and lowest and highest elevations (gray dashed lines) within a 50-km-wide swath along profile AA' in Figure 1a (vertical exaggeration 8:1). In its frontal part, the MHT has been slipping at 21 ± 1.5 mm/yr during the Holocene according to terraces warping across the Sub-Himalaya [*Lavé and Avouac*, 2000].

from structural observations [*Schelling and Arita*, 1991; *Schelling*, 1992] and seismological data [*Seeber and Armbuster*, 1981; *Pandey et al.*, 1995]. The midcrustal reflector imaged in a deep seismic cross section beneath south Tibet would correspond to the northward extension of the MHT [e.g., *Zhao et al.*, 1993] (Figure 2).

### 2.2. Active Tectonics in the Himalayas of Central Nepal and Its Relation to Present Topography

Evidence for recent deformation was found at various localities along the MFT, within the Sub-Himalaya, along the MBT or in the LH [*Nakata*, 1989; *Mugnier et al.*, 1994]. Recent investigations of active tectonics across the Lesser and Sub-Himalaya south of Kathmandu [*Lavé and Avouac*, 2000] show that the MFT is clearly the major active fault there. Indeed, slip along the MFT at 21 ± 1.5 mm/yr [*Lavé and Avouac*, 2000] absorbs nearly all the present shortening rate across the whole Himalayan range as estimated from GPS measurements [*Bilham et al.*, 1997; *Larson et al.*, 1999; *Jouanne et al.*, 1999]. Paradoxically, the highest Himalayan peaks lie parallel to the MFT but 100 to 150 km farther to the north and 20 to 50 km north of the trace of the MCT (Figures 1 and 2). The reason for this paradox remains unclear, and several explanations have been proposed.

Active thrusting in the upper crust along or close to the MCT might explain the present morphology of the front of the HH. This was argued, for example, by *Seeber and Gornitz* [1983] on the basis of the observation that seismic activity and river knickpoints also tend to follow the front of the high range. More recently, *Bilham et al.* [1997] have observed that the front of the high range also coincides with a zone of interseismic uplift. They proposed that part of this interseismic uplift might be unrecoverable and contribute to building the high range in the long term by pervasive thrust faulting in the upper crust around the MCT. Another solution is that the MHT steepens and makes a ramp beneath the high range, as suggested by the antiformal structure of the LH [*Schelling and Arita*, 1991] (Figure 2). The front of the high range would then be maintained by overthrusting over a midcrustal ramp. Accordingly, the total shortening across the range would equal that accommodated by slip along the MFT

and the pattern of active uplift would be primarily controlled by the geometry of the MHT at depth.

If we now consider that the pattern of erosion might not be in equilibrium with active rock uplift, other explanations are possible. *Harrison et al.* [1997] found evidence for late Miocene reactivation of the MCT and suggest that the front the high range would, in fact, reflect this reactivation. Finally, as already mentioned, it has also been proposed that the present topography could reflect the isostatic response to enhanced erosion of the edge of the Tibetan Plateau by a Late Cenozoic monsoon strengthening or by Quaternary glaciations [*Burbank*, 1992; *Masek et al.*, 1994; *Montgomery*, 1994]. In that case, the pattern of uplift across the Himalayas would not be related closely to the kinematics of active thrust faulting.

The determination of fluvial incision along the major rivers draining across the Himalayas and its relation to landscape denudation and to active tectonics might thus be used to discriminate between these different models of mountain building and late Cenozoic uplift of the high range.

### 2.3. Characteristics of the Studied Fluvial Systems

The Narayani and Sapt Kosi watersheds drain most of the Himalayas of central Nepal. They include several rivers cutting across the HH with headwaters on the Tibetan Plateau (Figure 1b). The base level of erosion is controlled by sedimentation and subsidence in the foreland. Upstream of Tribenighat (Figure 1b), where it enters the Ganga basin, the Narayani drains an area of 38,000 km$^2$. The Sapt Kosi watershed covers a much larger area of 60,000 km$^2$. The difference is essentially due to the fact that the Arun River, which belongs to the Sapt Kosi watershed, drains an area of more than 20,000 km$^2$ on the Tibetan Plateau.

All the rivers in the study area are cutting down into bedrock except locally in the Sub-Himalaya, across the Dun. We have studied six trans-Himalayan rivers within these two watersheds that are, from west to east, the Kali Gandaki, the Marsyandi River, the Buri Gandaki, the Trisuli River, the Sun Kosi, and the Arun River (Figure 1). In the LH the rivers are characterized by relatively even stream gradient and convoluted courses with large east-west trending deflections (Figure 1). Across the HH, all the rivers cut straight along narrow and steep N-S gorges. Three of them, the Kali Gandaki, the Trisuli River, and the Arun River, have upper reaches flowing along some of the major N-S graben of southern Tibet, the Thakkola, the Gyirong, and the Pum Qu grabens, respectively. They therefore extend much farther north than the other trans-Himalayan rivers (Figure 1). The six rivers considered here differ significantly as to their size, climatic, lithologic, and tectonic settings. This diversity offers some possibility of discriminating the roles played by the various factors involved in fluvial incision.

Although it does not cut across the entire range, we also consider below the Bagmati river because it provides useful tie points to assess terrace ages and for calibrating incision rates (Figure 1a).

## 3. River Incision as Recorded by Fluvial Terraces

We now investigate terrace records along the central Himalayan rivers. Across the Siwaliks, numerous dated terraces permit a precise quantification of fluvial incision rates and provide the basis for a relative dating of the terraces in the LH and HH.

### 3.1. Methodology for Estimating Long-Term Fluvial Incision Profiles

The simplest and most direct method for estimating river incision is to date and measure the elevation of former river beds with respect to the present river bed. Fortunately, fluvial terraces are ubiquitous in the Sub-Himalaya and LH of central Nepal. Following *Bull* [1991], we distinguish strath and fill terraces. Strath terraces are characterized by thin fluvial gravel (<10 m) over a subhorizontal level, the strath surface, carved into the bedrock by fluvial erosion. If the gravel is thicker than ~10 m, we call it a fill terrace.

The terraces in the study area were first recognized and mapped from air photographs, and Landsat and SPOT images. In the field they were classified according to their geomorphic nature, the facies of the fill material, degree of weathering, and thickness of the soil profile. Nearby disconnected treads were also correlated on the basis of their elevation. Elevations were measured with a digital altimeter that provides an error <10 m, when measuring the elevation of a terrace relative to the river and from 1:63,000 topographic maps with elevation contours every 30.5 m. Where possible, we measured elevations of the terrace tread, of the strath surface at the base of the fill and of the present river bed at the same location.

It might be assumed that the elevation of the top of the terrace tread above the present river bed is representative of the long-term average fluvial incision (see, for example, the analysis by *Molnar* [1987] of the terrace record measured by *Iwata et al.* [1984] along the Kali Gandaki). It may be of little importance in the case of a strath terrace with a thin veneer of gravel and silt. It is more problematic when the gravel cap has a thickness comparable to the elevation of the terrace above the present river bed. This is because, as shown schematically in Figure 3, river incision is far from monotonous. In active mountainous regions, reincision of alluvial or noncohesive materials is usually more rapid than bedrock incision because sediments offer much less resistance to erosion than bedrock. Let us assume that at stage 1 the river flows on the bedrock and that an episode of fluvial aggradation takes place between stages 1 and 2 (it may result from transient fluvial response to a climatic change [e.g., *Bull*, 1991; *Weldon*, 1986] or from a catastrophic mud flow or debris flow). River incision proceeds rapidly into the fill material until the surface of previous strath is reached. This surface has been gradually uplifted between stages 1 and 3 while protected from further erosion by the gravel cap. Between stages 3 and 4, bedrock is exposed and the river may cut into it until the next filling event. In such a case, the long-term incision rate $i_{LT}$ (Figure 3) cannot easily be measured because it corresponds to mean bedrock incision rate $i_b$ weighted by the relative time of bedrock exposure to mechanical erosion $\Delta t_{exp}/\Delta t$ :

$$i_{LT} = i_b \, \Delta t_{exp} / \Delta t \, . \qquad (1)$$

In the Siwaliks we did not see any thick gravel [*Lavé and Avouac*, 2000], and reincision of this material is rapid. In that case, the long-term incision rate is roughly equal to mean bedrock incision rate.

Such a composite history, with possibly several successive episodes of strath abrasion, fill deposition, reincision, and

downcutting into the bedrock, might only be partially reconstructed from a terrace survey. River incision derived from the elevation and age of strath surfaces (comparison of stages 1 with present river bed, for example) is probably the most reliable estimate of long-term averaged incision rate. Unfortunately, the strath surface beneath a fill terrace is often difficult to find (stage 3b) because a river does not systematically reincise its former valley along the same vertical axis (hereinafter referred to as epigenetic valley). The elevation of the bedrock beneath the fill then only provides an upper bound on the amount of river incision into the bedrock since stage 1. Moreover, the age of strath terrace formation (stage 1) is underestimated if it comes from dating of samples within the fill deposit. We might therefore overestimate the long-term averaged rate of river incision. The overestimation is even worse if river incision is derived from the age and elevation of a fill terrace tread. Conversely, if the present river has only recently reexposed bedrock (stage 3), as is often observed in the LH, long-term incision rate may be underestimated when derived from the strath surface. With these limitations in mind, we will discuss hereinafter incision rate profiles along the major Himalayan rivers.

### 3.2. Fluvial Terraces in the Sub-Himalaya

Fluvial terraces have already been extensively surveyed in the Sub-Himalaya of central Nepal, in particular along the Bagmati, Bakeya, Narayani, and Ratu rivers [*Delcaillau*, 1992; *Lavé and Avouac*, 2000]. The investigated sites are shown in Figure 1a. The $^{14}C$ dating of these terraces has revealed four major episodes of strath terrace formation (Table 1) [*Lavé and Avouac*, 2000]. The uppermost level, labeled $T_0$ and dated at ~9.2 calendar (cal.) kyr B.P., corresponds to particularly wide terrace treads. The second most prominent level is $T_3$ (dated at 2.2 cal. kyr B.P.). The strath surfaces are generally covered by a few meter thickness of gravel, overlain by overbank sands and silts. These Holocene terraces are characterized by a low degree of weathering with a beige to orange color of the silt and sand. Along the Bagmati (Figure 4), the age control could be checked since the obtained chronology was found to be consistent with the relative degree of warping recorded by the various terrace treads that could be followed across the rising anticline associated with the MFT [*Lavé and Avouac*, 2000]. Similar results have been obtained along the Bakeya River, which cuts across the same anticline 40 km to the west of the Bagmati and is characterized by a much smaller watershed (280 km$^2$) [*Lavé and Avouac*, 2000].

Pleistocene terraces have also been encountered locally along the rivers cutting the rising anticlines but are mostly preserved along the Duns (Figure 4) where uplift rates, and hence denudation rates, are subdued. So far, there has been no direct dating of these terraces, which are characterized by more intense weathering so that organic material is generally not preserved. According to their degree of weathering, they can be divided into three families, $Pl_3$, $Pl_2$, and $Pl_1$, along the Bagmati (Table 1). Assuming a constant late Quaternary rate of folding at the MFT, the deformation profiles [*Lavé and Avouac*, 2000] associated with each terrace tread can be used to estimate its age of formation (Table 1). In the following, we use this classification based on weathering profile in the Bagmati valley to estimate age of formation of the terraces in

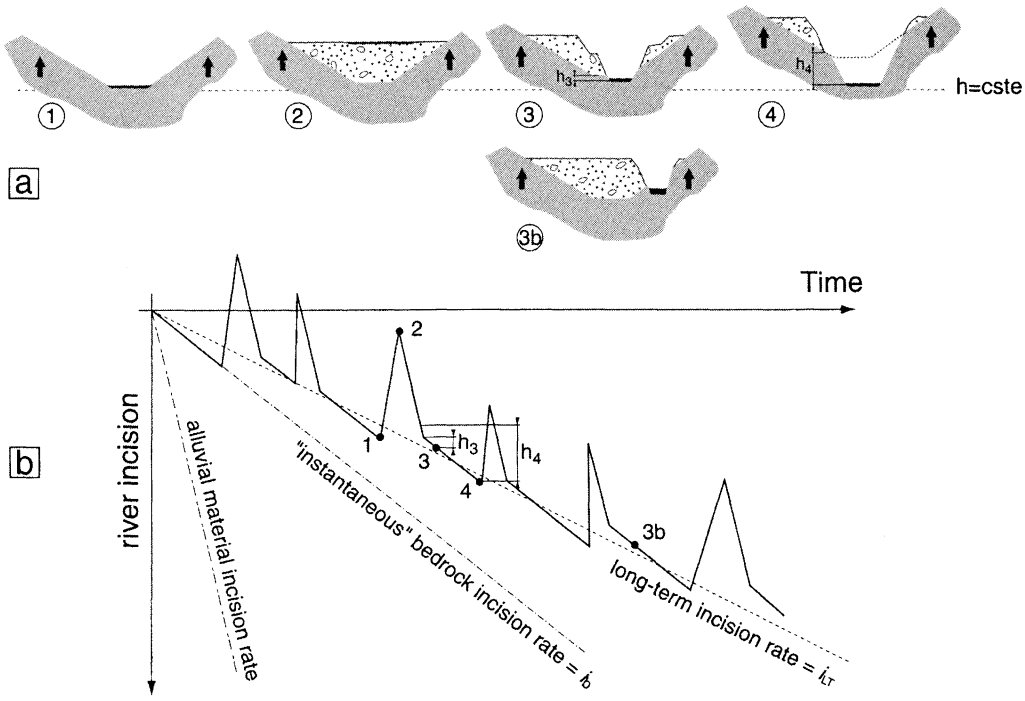


**Figure 3.** History of river incision and fluvial aggradation in a valley submitted to a regional uplift rate. (a) Schematic profiles at different stages and (b) the time evolution. At stage 1 the river flows on the bedrock and incises. A transient episode of fluvial aggradation takes place between stages 1 and 2 (for example, as a result of internal adjustment of the fluvial system to a changing climate). River incision is rapid into the fill material until the previous strath is reached at stage 3, or 3b in case of epigenetic valley (see definition in the text). At stage 4 the river has cut into the bedrock at its maximum erosive capacity until the next filling event. The long-term incision rate results from two distinct phases and therefore is lower than the "instantaneous" bedrock incision rate. For simplicity, temporary pauses during reincision of the fill terrace material that could lead to the formation of fill cut terraces were not represented in this scheme.

the LH below 1000 m, where precipitation and temperature are roughly similar to Sub-Himalayan conditions.

### 3.3. Fluvial Terraces in the Lesser and Higher Himalaya

**3.3.1. Fluvial terraces along the Arun River.** The Arun River cuts across the entire Himalayan range of eastern Nepal along a roughly straight north-south course and joins with the Sun Kosi and Tamur rivers to form the Sapt Kosi (Plate 1). Our field survey has revealed that the terraces along the lower reach present strath levels analogous to those surveyed in the Sub-Himalaya. North of the Tamur Kosi Thrust (TKT), a nearly continuous tread lies ~40 m above present river bed (apr) and has probably been warped and uplifted by ~20 m (Plates 2a and 3a). A 20-m-thick gravel caps a strath surface beveled into the Paleozoic resistant bedrock. The strath surface has been warped and uplifted by the same amount as the tread at the top of the fill, suggesting that the fill resulted from a relatively brief episode of aggradation. The bottom of the fill consists of 10-15 m of submetric to metric boulders, including bedload material and some sparse 2-3 m angular blocks of local origin. This material fines upward to 10 m of sands to silts. A charcoal sample (MACH-5 in Plate 3a) was found in a sandy lens at the top of the bedload layer. It places an upper bound of ~9.1 kyr cal. B.P. [*Lavé*, 1997] for the abandonment of the strath surface. This strath thus appears to correspond to the $T_0$ level recognized along the Bagmati and Bakeya Rivers. The geometry of the terrace tread suggests that active uplift near the TKT has forced the river to entrench by up to 2.5 mm/yr (Plate 3a).

Along the middle reach of the Arun River (near Tumlingtar in Plate 1), the terraces are very much like the fill terraces described elsewhere in the LH [*Fort*, 1993; *Iwata et al.*, 1984]. For example, the prominent terraces at the confluence with the Sama Khola near Tumlingtar are particularly typical. Two terraces treads, $Ft_1$ and $Ft_2$, can be distinguished there that lie ~100 m and 150 m apr, respectively (Plate 3a). They may form two inset fill terraces, or the second terrace may have been cut into the fill of the upper one. The present river has cut down through the entire fill and, south of Tumlingtar, into the underlying bedrock by around 15 m. This is a maximum estimate since no clear strath level could be observed. The terrace tread at 150 m apr is deeply weathered, with a soil profile over 5 m thick. The top of the fill consists of mixed boulders, sand, and gravel with no layering. It contains angular blocks of up to 2 m in diameter. The 100-m-high terrace tread is less deeply weathered (2-m-thick red soil). The fill material below contains some layered gravel and mostly a coarse sandy matrix with sparse metric blocks of LH schist. The degree of weathering on these terraces, compared with the terraces in the Sub-Himalaya where a more humid and warmer climate should favor a more rapid rate of weathering, suggests that $Ft_2$ terraces were probably abandoned before 15 kyr B.P.. Since then, the Arun river has cut down by ≤15 m into the bedrock below the late Pleistocene fill at Tumlingtar, and long-term rates of fluvial incision probably do not exceed 1 mm/yr.

We have surveyed all the terrace remnants along the Arun River up to the gorges into the HH, where they were not preserved or never formed. Facies and elevations provide the

**Table 1.** Estimated Ages of Emplacement of the Terraces Considered in This Study[a]

| Sub-Himalaya (Bagmati and Bakeya) | | | Kali Gandaki | | Marsyandi | | Trisuli | Arun |
|---|---|---|---|---|---|---|---|---|
| Terrace Level | Formation Age, kyr B.P. | Upper Weathering Profile | Lower | Upper | Lower | Upper | | |
| | | | | *Holocene* | | | | |
| $T_3$ | (2.2)±0.2 | - | L | L | L<br>L' | | $T_3$ | $T_3$ |
| $T_2$ | (3.7)±0.1 | - | | $M_4$ | M'<br>M ((4.8) kyr) | $G_3$ | | |
| $T_1$ | (6.1)±0.2 | light orange weathering profile | | $M_2$ | | | $T_1$ | $T_{0fc}$ |
| $T_0$ | (9.2)±0.2 | orange weathering profile | | $M_1$ | | | $T_0$<br>((9.0) kyr) | $T_0$<br>((9.2) kyr) |
| | | | | *Pleistocene* | | | | |
| HPl | 10-15 | deep orange red weathering profile = 1 m | $M_5$<br>$M_4$<br>$M_3$ | | | $Ft_3$ | HPl | $Pl_3$ |
| $Pl_3$ | 15-30 | 1 m > red weathering profile > 3 m | $M_2$<br>$M_1$ | | | $G_2$ | $Ft_2$ | $Ft_{2fc}$<br>$Ft_2$ |
| $Pl_2$ | 30-50 | 3 m > red weathering profile > 5 m | H | H<br>(60>age> 35 kyr) | H | | $Ft_{2'}$ | |
| $Pl_1$ | > 45 | red weathering profile > 5 m | | | HH | | $Ft_1$ | |

[a]Chronology of the Sub-Himalayan Holocene terraces has been established from charcoal dating (parentheses); chronology of the Sub-Himalayan Pleistocene terraces was derived by comparing their warping with that of well-dated Holocene terraces assuming constant uplift rate; chronology of the terraces along rivers draining the LH was inferred by comparing weathering profiles with those of the Sub-Himalayan rivers and some sparse dating (parentheses, see text for references).

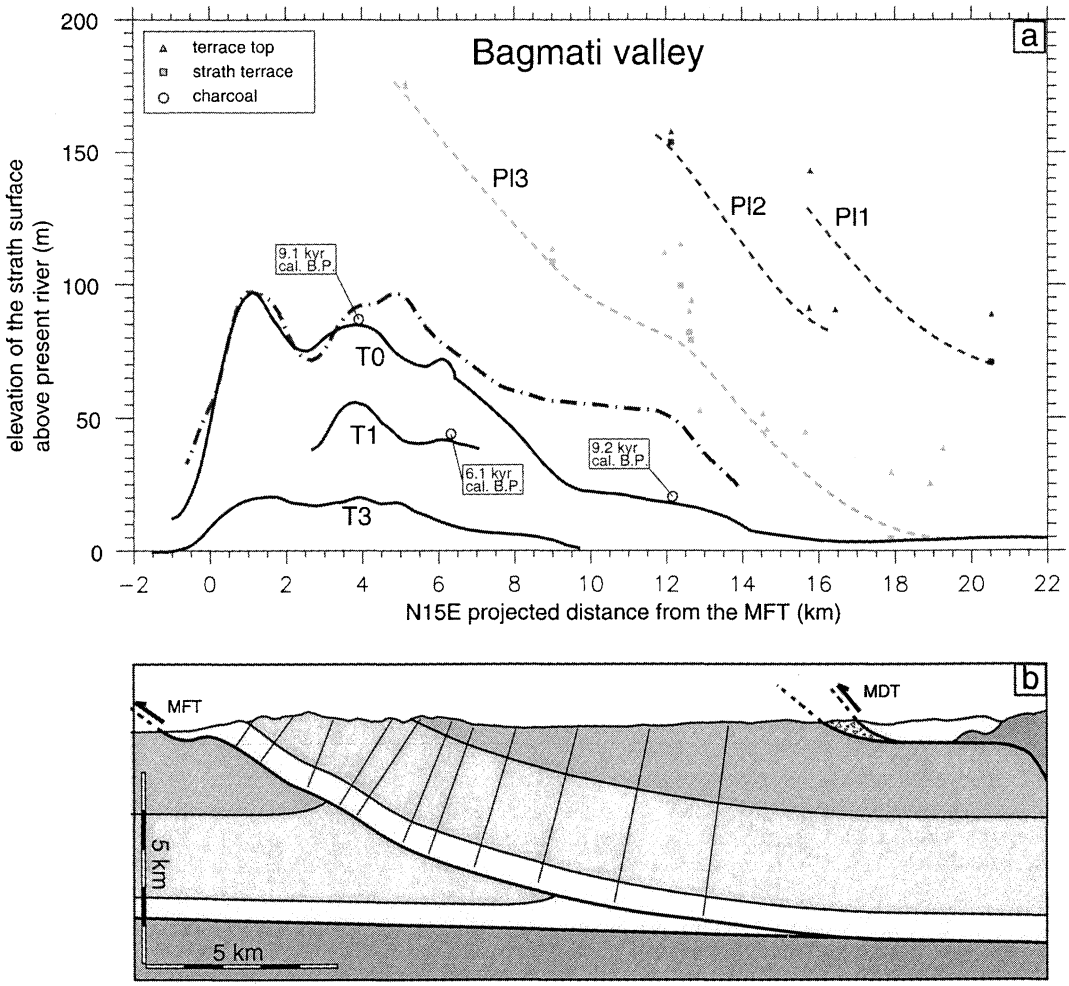


**Figure 4.** (a) Elevation above present river bed, along a N15°E profile (profile BB' in Figure 1a), of the strath surfaces recognized along the Bagmati River (Holocene terraces in bold lines, undated Pleistocene terraces in dashed line). The sites where good chronological control could be obtained from $^{14}C$ dating of charcoal fragments are also reported [*Lavé and Avouac*, 2000]. (b) Theoretical uplift profile (dash-dotted line in Figure 4a) derived from the structural section assuming fault bend folding at the MFT [*Lavé and Avouac*, 2000].

basis for an attempt at correlation (Plate 3a). River incision into the bedrock beneath the fill terraces appears to increase upstream, suggesting a larger amount of fluvial incision at the front of the HH where the river gradient rises abruptly (Plate 2a, lower dashed orange line in Plate 3a). The relatively abrupt break in slope of the terrace tread at km 65 (Plate 3a) might be taken to reflect some warping as well, but such a conclusion is highly speculative and dependent on the initial geometry of the terrace tread. More generally, because of the difficulty in assessing ages and amounts of fluvial incision and in correlating the various terrace treads, the terrace record in the LH thus only provides qualitative information.

**3.3.2. Fluvial terraces along the Trisuli.** In its lower reach the Narayani River cuts across the Sub-Himalayan range along the MFT just north of Tribenighat (Figure 1b). There, some strath terraces similar to those along the Bagmati and Bakeya Rivers were identified and investigated in the field. Two terraces were dated from charcoal samples: the highest one is early Holocene at 9.2 cal. kyr B.P. and the second corresponds to a meander abandoned at 2.7 cal. kyr B.P. [*Lavé*, 1997]. Both samples indicate consistent incision rates of 6-7 mm/yr. As along the Bagmati River, fluvial incision has been forced by active thrusting at the MFT. MDT activity has also been observed from a terrace study by *Iwata and Nakata* [1986] north of Naryanghat at the confluence between Kali and Trisuli (Plates 2b, 3b, and 4). According to our observation on the weathering profile of these terraces, *Iwata and Nakata*'s [1986] terrace level V may have formed during the early Holocene. Strath elevation (~25 m) of this terrace level would indicate an incision rate around 2-3 mm/yr.

In the LH the pattern is similar to that along the Arun River with major Pleistocene fill terrace at confluence basins (Plate 4). Two prominent Pleistocene treads can be distinguished both with >120 m fill material of dominantly fluvial origin. Numerous minor Pleistocene and Holocene fill-cut terraces and lateral fans form generally unpaired and disconnected remnants that cannot be correlated easily. The prominent terrace $Ft_1$, well exposed at the confluence with the Tadi Khola near Trisuli Bazaar (Plate 5a), displays a 10-m-thick

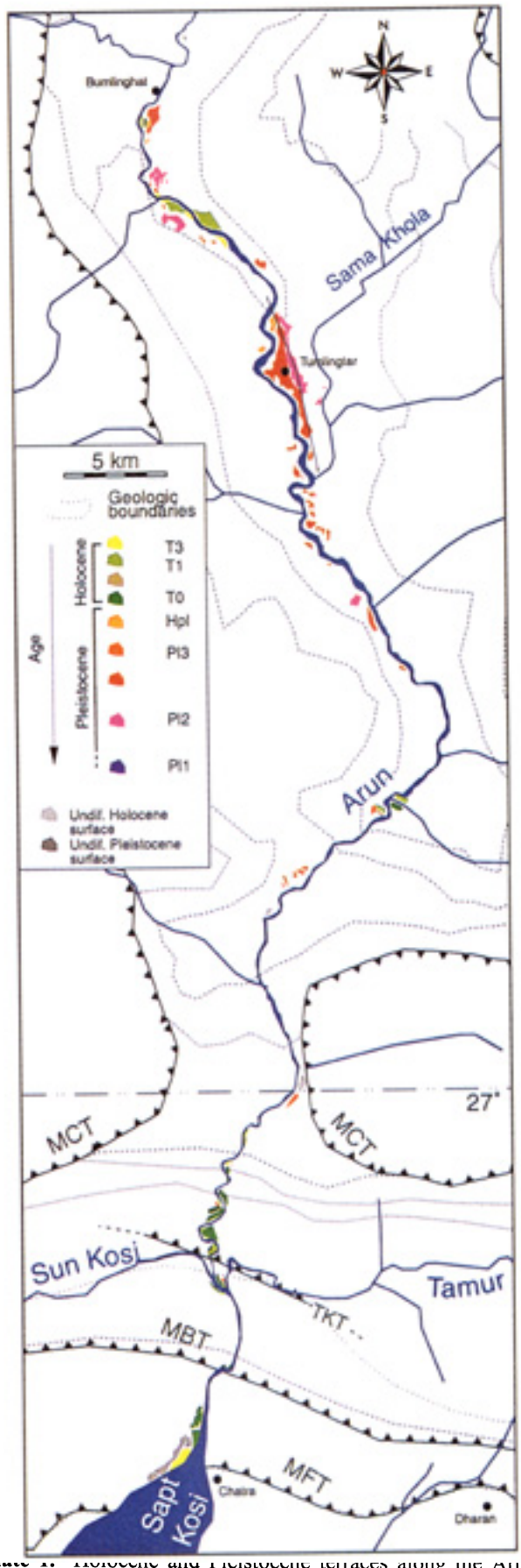


Plate 1. Holocene and Pleistocene terraces along the Arun River. See box in Figure 1a for location. TKT, Tamur Kosi Thrust.

weathering profile, indicative of an age probably older than 45 kyr (Table 1). At this locality the Tadi Khola has incised by <10 m into bedrock below the $Ft_1$ fill terrace, indicating an incision rate lower than ~0.25 mm/yr since $Ft_1$ was deposited. From Simpani to the Seti Khola confluence, some narrow strath terraces (usually <20 m wide) of presumably Holocene age have been observed. These terraces, which lie at distances between 20 and 30 km from the MFT (Plate 3b), suggest a more rapid incision rate along the river reach that flows around the western end of the Mahabarat.

North of Trisuli Bazaar, a systematic rise in the elevation of the terrace treads going upstream into the high range suggests some warping (Plate 3b). No terraces are preserved along the narrow gorge farther upstream.

**3.3.3. Fluvial terraces along the Marsyandi.** The Marsyandi River originates north of the Annapurnas massif. It cuts straight through the high range between Annapurna IV and Himal Chuli peaks. The river is more sinuous in the LH where abundant terraces are preserved, especially between Besi Sahar and Dhumre (Plate 4). *Yamanaka and Iwata* [1982] already surveyed this area and identified four main levels, labeled HH, H, M, and L (Table 1). The fill terrace level H is well preserved and can be followed throughout the LH from Dhumre up to Besisahar along the Marsyandi and most tributaries. The fill material consists of mixed fluvial and debris flow units with some organic rich clay lenses. Deep red weathering of the soil over a thickness of 4 m suggests an age older than ~30 kyr. The elevation of the terrace top slightly decreases downstream from 130 to 95 m apr. At Tharkughat the contact between the fill and the bedrock lies only a few meters above present river, suggesting an incision rate lower than 0.3 mm/yr.

The intermediate terrace M is a mudflow deposit fed from the high range dated to 4.3 kyr B.P. (4.8 cal kyr B.P. in Plate 3c) [*Yamanaka and Iwata*, 1982]. Near Tharkughat, the river has reincised the mudflow deposit, leaving fill cut terraces (including terrace level L) but has not yet reached the previous valley bottom, except locally due to epigenetic valley. Although the correlation is speculative, this mudflow deposit can be traced upstream until the village of Jagat (Plate 4). There, the river has cut through the mudflow deposit and <30 m into the underlying bedrock. The incision rate thus appears to increase upstream as the river approaches the front of the high range with, at Jagat, a rate of 6 mm/yr or less. Across the high range the river drains along a steep and narrow gorge with very few preserved terraces between Besi Sahar and Bagarchap, except numerous lateral figures of fluvial erosion carved into the canyon walls.

North of the Annapurna massif the Marsyandi River gets wider and less steep. Ubiquitous geomorphic relics indicate subdued river incision (Plates 2c and 4). These geomorphic features mainly consist of remnants of frontal and lateral moraines overhanging the present river bed by up to 400 m (Plate 3c). The river has generally not entrenched significantly deeper than the base of these deposits, which most probably relate to the Last Glacial Maximum (LGM) [*Fort*, 1993]. Altogether these observations suggest little river incision north of the Annapurna massif.

A 400-m-high moraine remnant in Naje (Plates 3c and 4), with a bedrock level at 360 m apr, however, might attest to important bedrock incision. If this moraine was formed during the LGM, it would suggest a dramatic drop in bedrock incision rate over 10 km. Alternatively, this remnant may

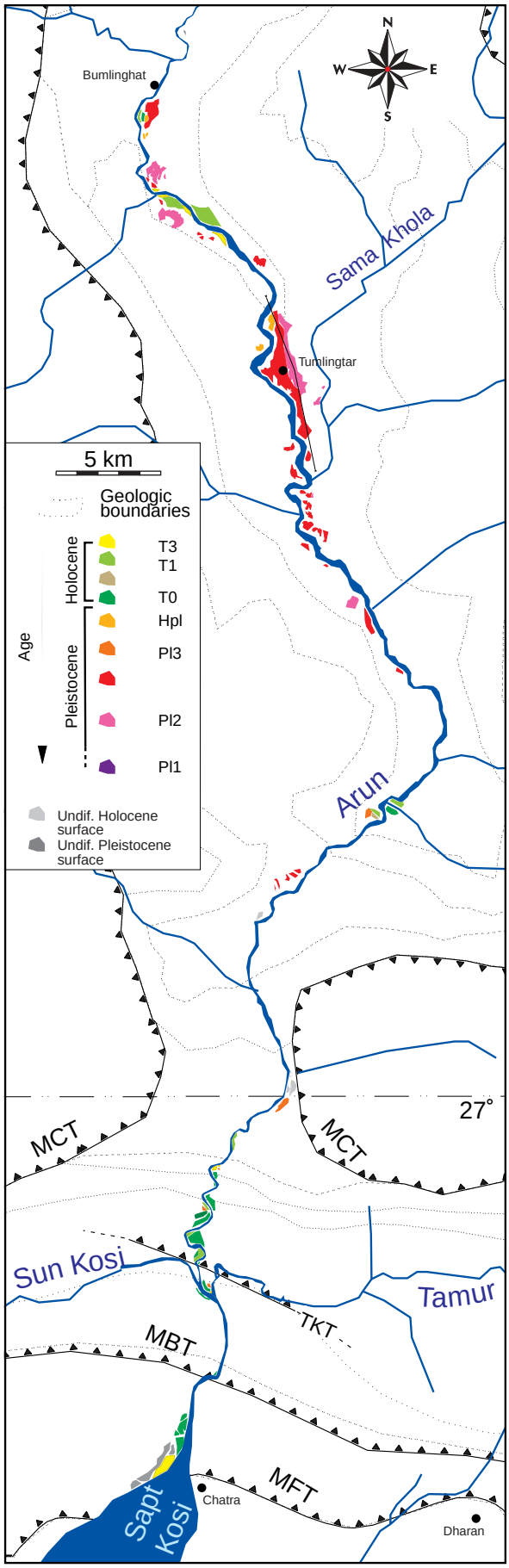
N
W
E
S
Bumlinghat
Sama Khola
Tumlingtar
5 km
Geologic boundaries
Age
Holocene
Pleistocene
T3
T1
T0
Hpl
Pl3
Pl2
Pl1
Undif. Holocene surface
Undif. Pleistocene surface
Arun
27°
MCT
MCT
Sun Kosi
Tamur
TKT
MBT
MFT
Sapt Kosi
Chatra
Dharan

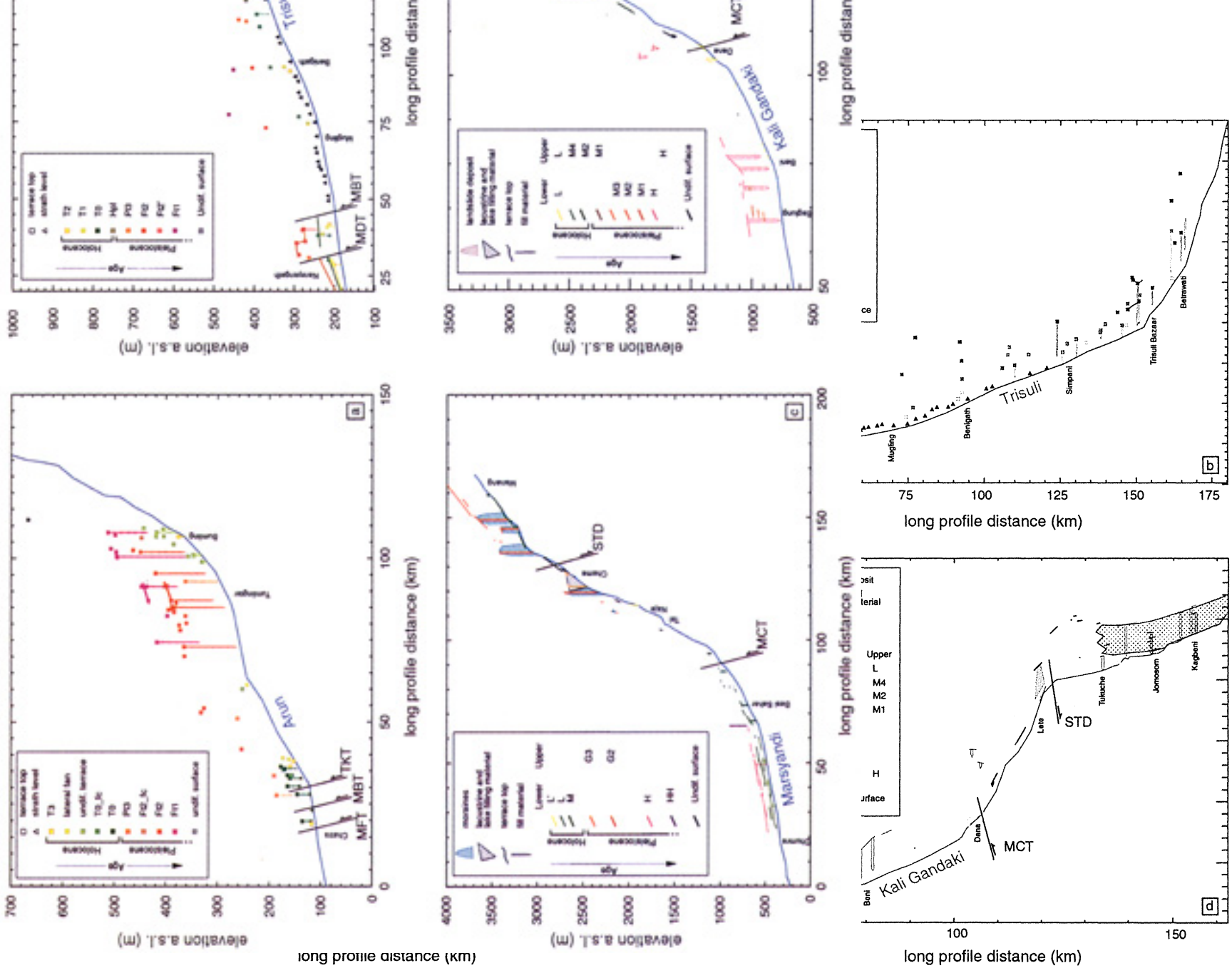


**Plate 2.** Longitudinal elevation profiles of present river bed (blue line), terrace treads and moraines along (a) Arun, (b) Trisuli, (c) Marsyandi, and (d) Kali Gandaki. Elevation of the top of the terraces is indicated by squares or color lines for extensive continuous surfaces, strath surfaces by triangles, and minimum thickness of the fill by vertical bars. Note different scales of panels.

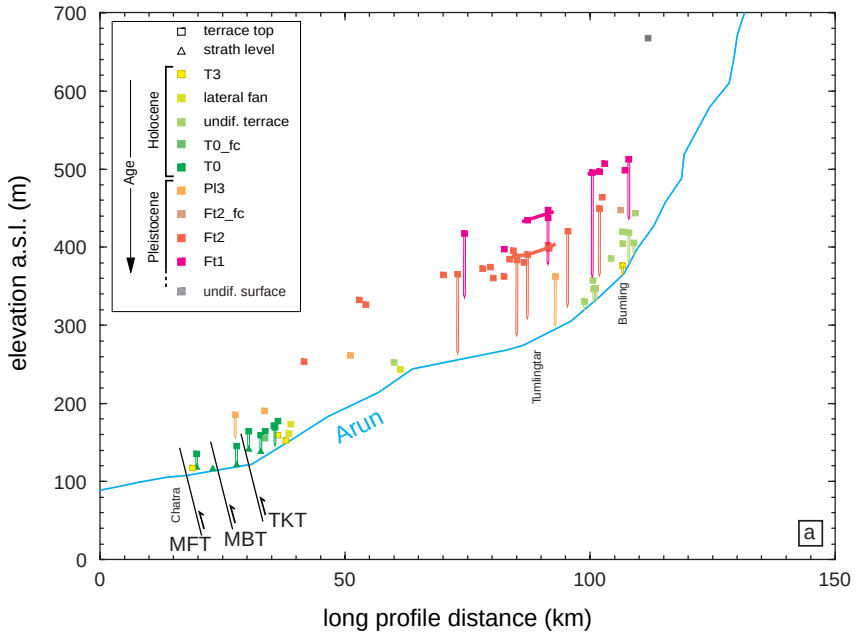
terrace top
strath level
Age
Holocene
T3
lateral fan
undif. terrace
T0_fc
T0
Pleistocene
Pl3
Ft2_fc
Ft2
Ft1
undif. surface
elevation a.s.l. (m)
long profile distance (km)
Arun
Chatra
Tumlingtar
Bumling
MFT
MBT
TKT
a

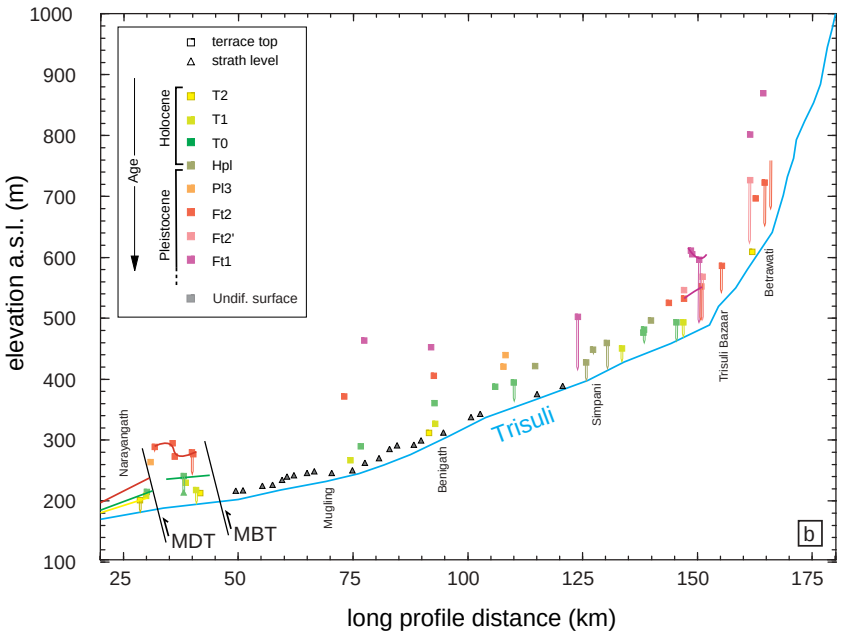
terrace top
strath level
Age
Holocene
T2
T1
T0
Hpl
Pleistocene
Pl3
Ft2
Ft2'
Ft1
Undif. surface
elevation a.s.l. (m)
long profile distance (km)
Trisuli
Narayangath
Mugling
Benigath
Simpani
Trisuli Bazaar
Betrawati
MDT
MBT
b

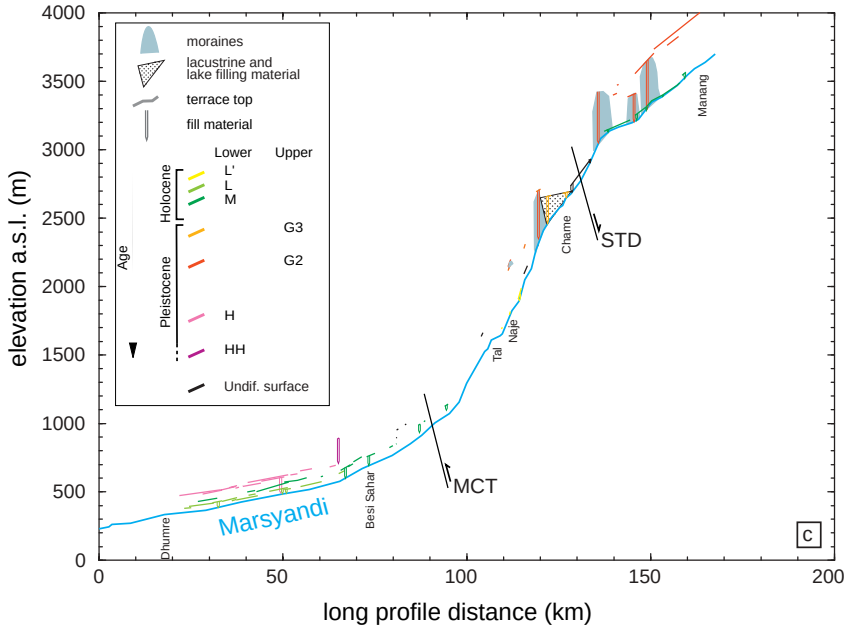
moraines
lacustrine and lake filling material
terrace top
fill material
Lower
Upper
Age
Holocene
L'
L
M
Pleistocene
G3
G2
H
HH
Undif. surface
elevation a.s.l. (m)
long profile distance (km)
Marsyandi
Dhumre
Besi Sahar
Tal
Naje
Chame
Manang
MCT
STD
c

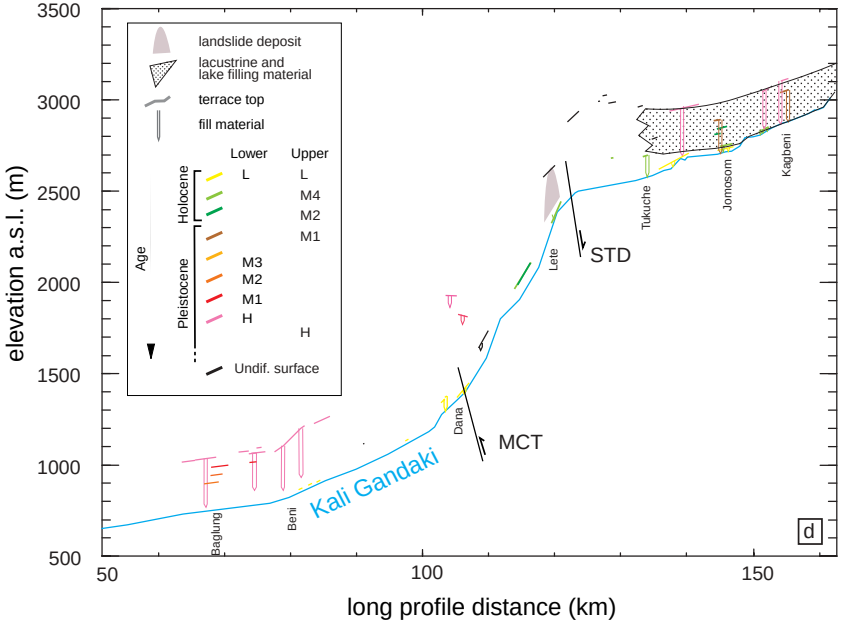
landslide deposit
lacustrine and lake filling material
terrace top
fill material
Lower
Upper
Age
Holocene
L
L
M4
M2
M1
Pleistocene
M3
M2
M1
H
H
Undif. surface
elevation a.s.l. (m)
long profile distance (km)
Kali Gandaki
Baglung
Beni
Dana
Lete
Tukuche
Jomosom
Kagbeni
MCT
STD
d

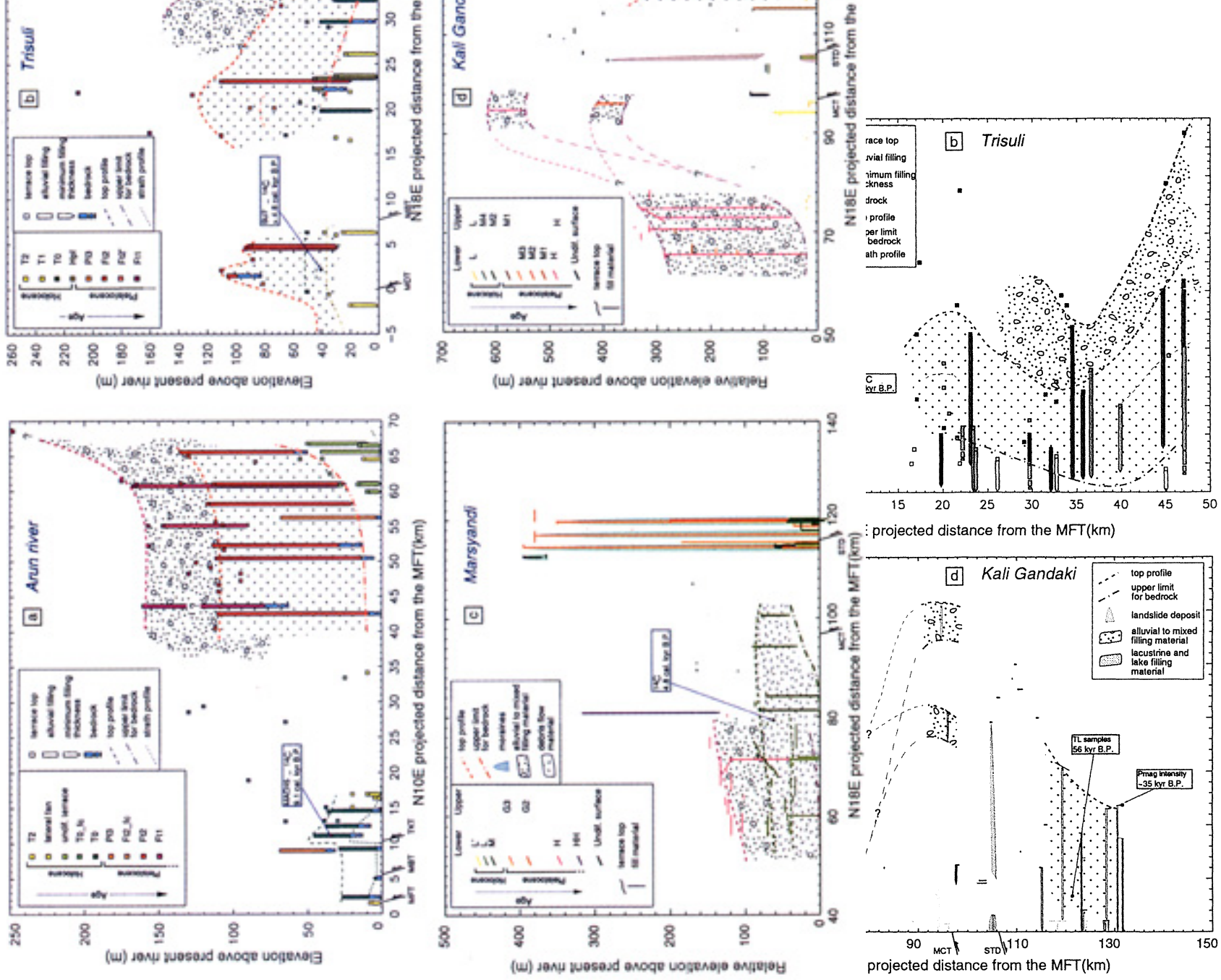


**Plate 3.** Elevations above present river bed of the various terrace treads and moraines along (a) Arun, (b) Trisuli, (c) Marsyandi, and (d) Kali Gandaki with the proposed correlation (dashed lines). The bedrock level indicates maximum elevation of the valley floor, providing an upper bound on fluvial incision since the filling of the paleovalley. Dates have been also reported for some terraces (see text for references).

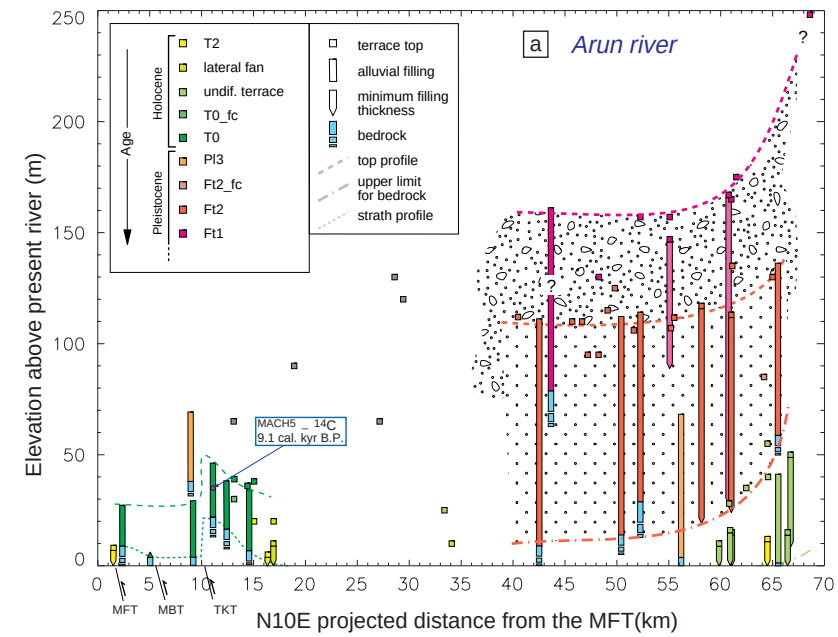
a
Arun river
Age
Holocene
Pleistocene
T2
lateral fan
undif. terrace
T0_fc
T0
Pl3
Ft2_fc
Ft2
Ft1
terrace top
alluvial filling
minimum filling thickness
bedrock
top profile
upper limit for bedrock
strath profile
MACH5 _ 14C
9.1 cal. kyr B.P.
Elevation above present river (m)
MFT
MBT
TKT
N10E projected distance from the MFT(km)

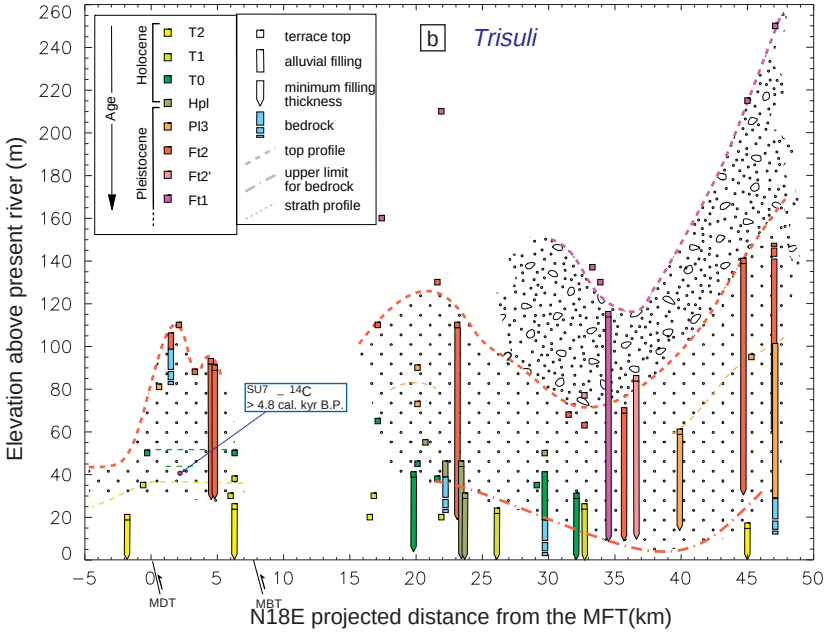
b
Trisuli
Age
Holocene
Pleistocene
T2
T1
T0
Hpl
Pl3
Ft2
Ft2'
Ft1
terrace top
alluvial filling
minimum filling thickness
bedrock
top profile
upper limit for bedrock
strath profile
SU7 _ 14C
> 4.8 cal. kyr B.P.
Elevation above present river (m)
MDT
MBT
N18E projected distance from the MFT(km)

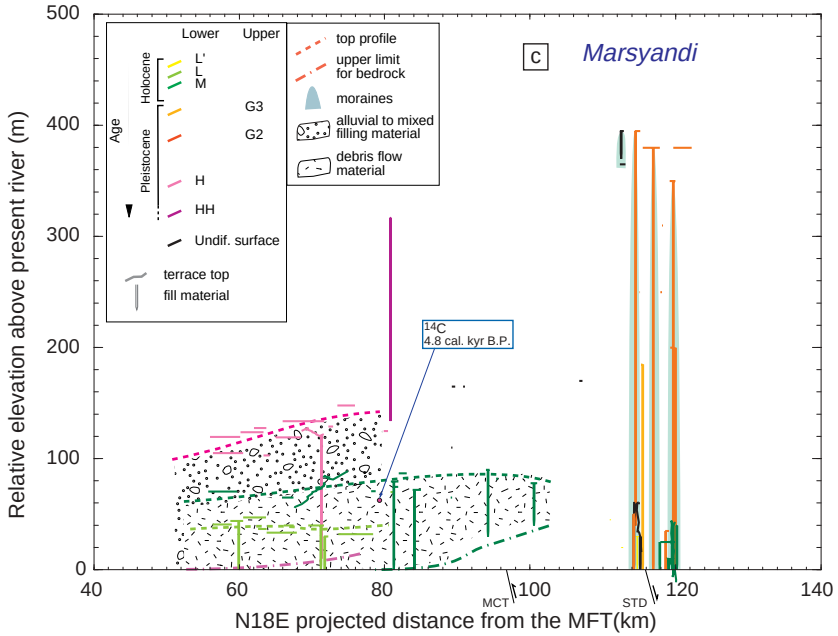
c
Marsyandi
Age
Holocene
Pleistocene
Lower
Upper
L'
L
M
G3
G2
H
HH
Undif. surface
terrace top
fill material
top profile
upper limit for bedrock
moraines
alluvial to mixed filling material
debris flow material
14C
4.8 cal. kyr B.P.
Relative elevation above present river (m)
MCT
STD
N18E projected distance from the MFT(km)

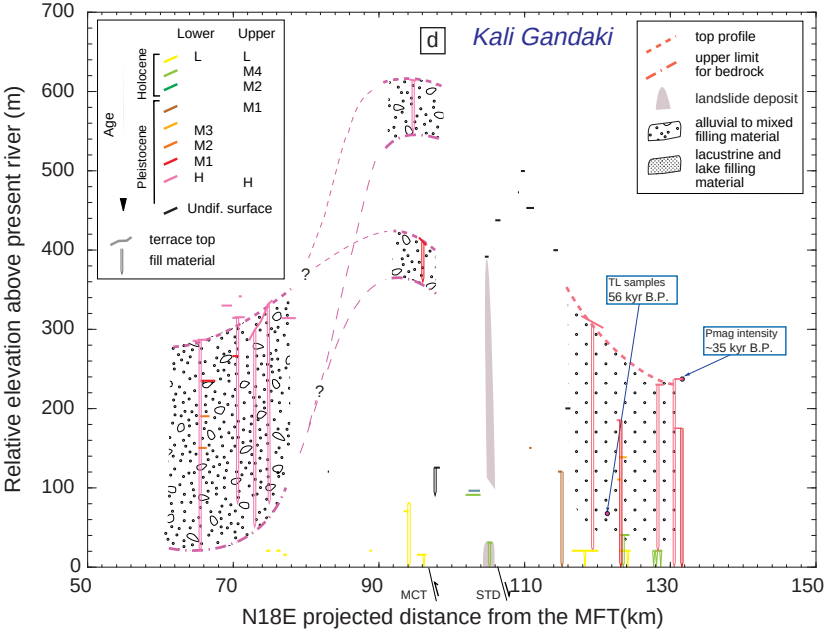
d
Kali Gandaki
Age
Holocene
Pleistocene
Lower
Upper
L
L
M4
M2
M1
M3
M2
M1
H
H
Undif. surface
terrace top
fill material
top profile
upper limit for bedrock
landslide deposit
alluvial to mixed filling material
lacustrine and lake filling material
TL samples
56 kyr B.P.
Pmag intensity
~35 kyr B.P.
Relative elevation above present river (m)
MCT
STD
N18E projected distance from the MFT(km)

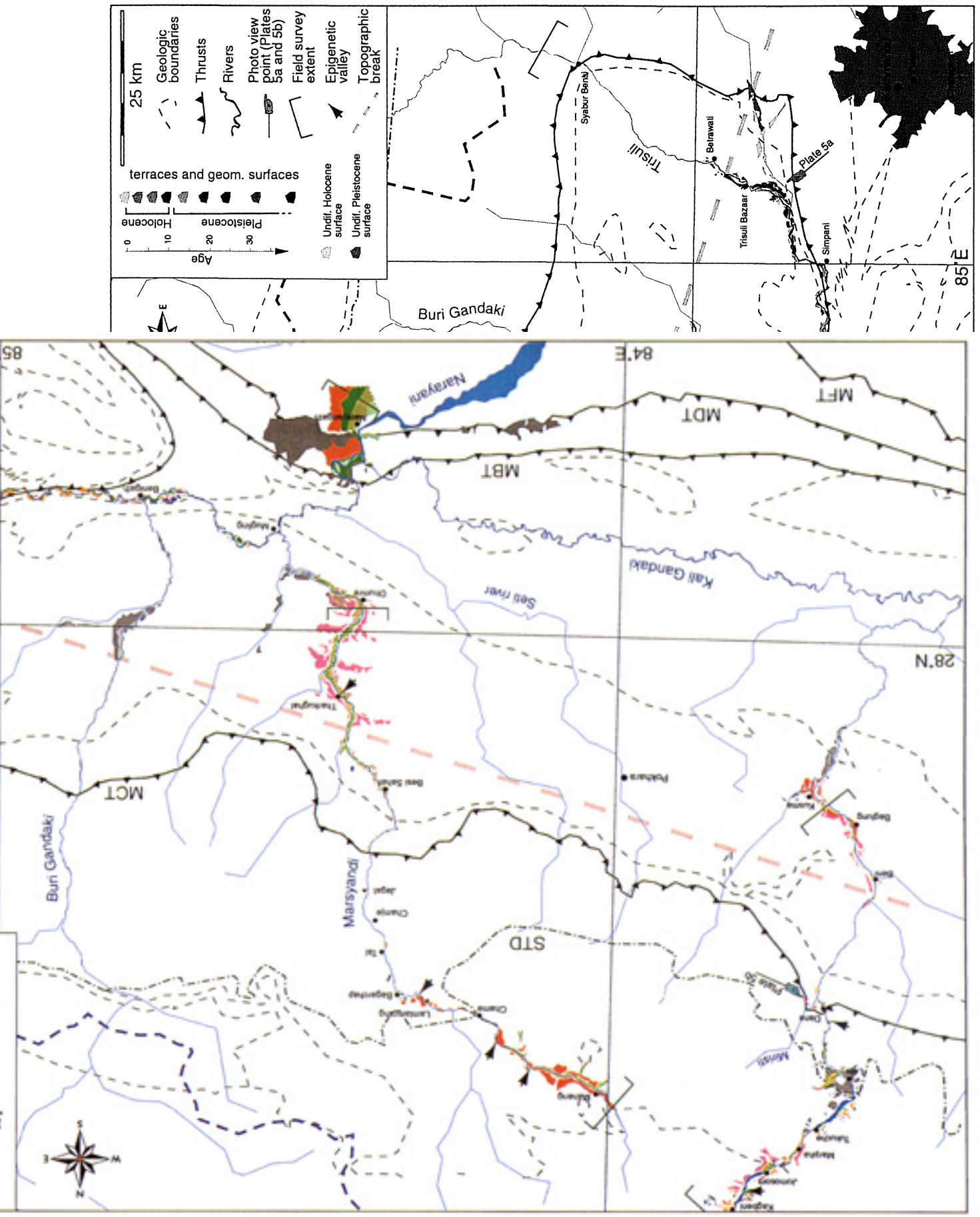
25 km
Geologic boundaries
Thrusts
Rivers
Photo view point (Plates 5a and 5b)
Field survey extent
Epigenetic valley
Topographic break
terraces and geom. surfaces
Holocene
Pleistocene
Age
0
10
20
30
Undif. Holocene surface
Undif. Pleistocene surface
Syabur Bensi
Trisuli
Betrawati
Plate 5a
Trisuli Bazaar
Simpani
85°E
Buri Gandaki
Narayani
MBT
MDT
MFT
Kali Gandaki
Seti river
28°N
MCT
Buri Gandaki
Marsyandi
STD
84°E
85

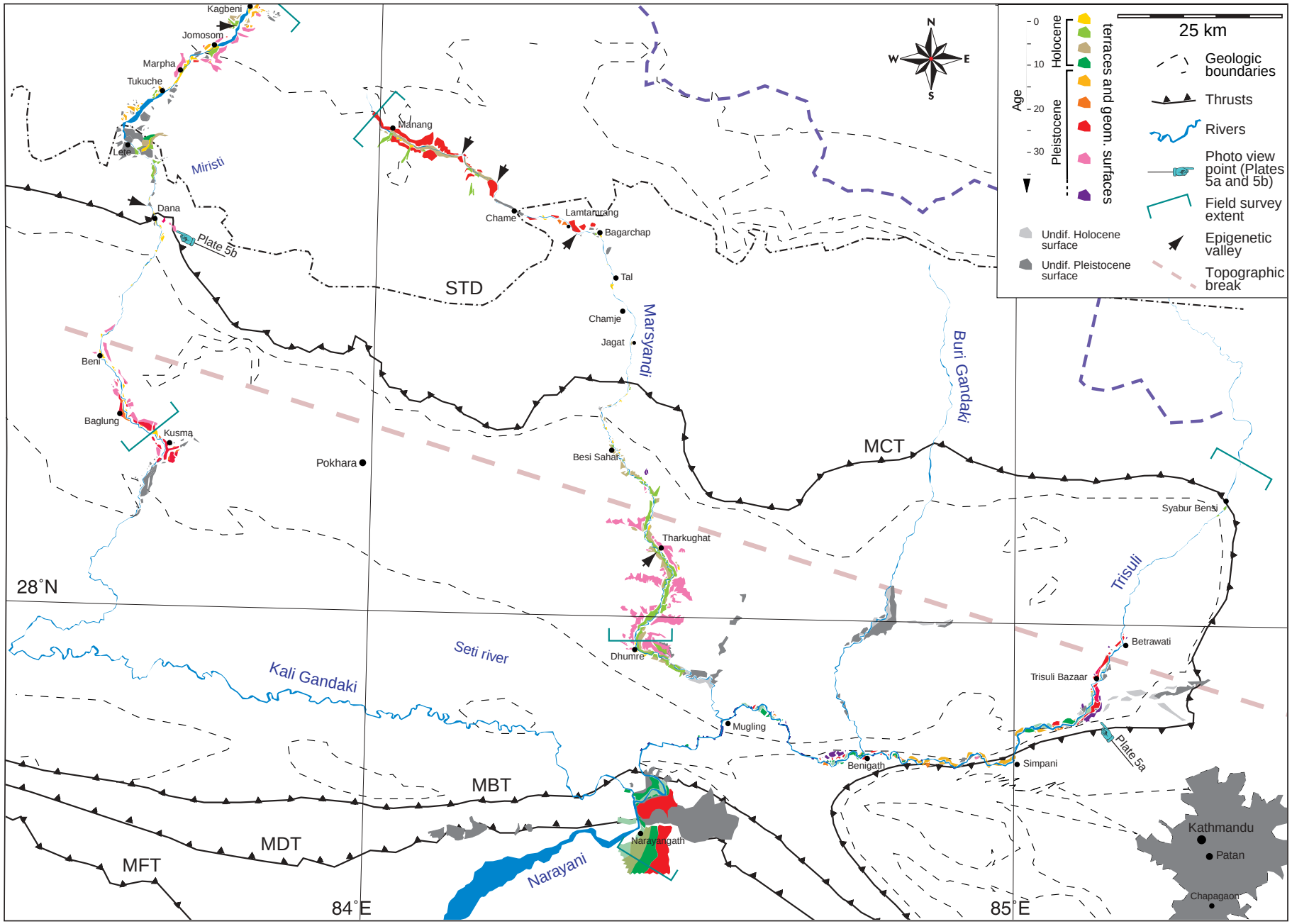
Kagbeni
Jomosom
Marpha
Tukuche
Lete
Miristi
Dana
Plate 5b
Manang
Chame
Lamtangrang
Bagarchap
Tal
Chamje
Jagat
Marsyandi
STD
Beni
Baglung
Kusma
Pokhara
Besi Sahar
MCT
Buri Gandaki
Tharkughat
Dhumre
Syabur Bensi
Trisuli
Betrawati
Trisuli Bazaar
Plate 5a
Simpani
Benigath
Mugling
Seti river
Kali Gandaki
MBT
MDT
MFT
Narayangath
Narayani
Kathmandu
Patan
Chapagaon
28˚N
84˚E
85˚E
N
S
W
E
Age
0
10
20
30
Holocene
Pleistocene
terraces and geom. surfaces
Undif. Holocene surface
Undif. Pleistocene surface
25 km
Geologic boundaries
Thrusts
Rivers
Photo view point (Plates 5a and 5b)
Field survey extent
Epigenetic valley
Topographic break

correspond to an older glacial maximum. In any case, this example illustrates the general difficulty in estimating the incision rate in previously glaciated valleys, where the profile of a paleovalley shaped by the glaciers does not present any geomorphic equivalence with the present river profile.

**3.3.4. Fluvial terraces along the Kali Gandaki.** The terraces along the Kali Gandaki have attracted much attention [*Fort*, 1993; *Iwata et al.*, 1982, 1984; *Kuhle*, 1982], but their chronology remains largely unconstrained. In the LH, an up to 300-m-thick fill terrace, labeled H by *Yamanaka and Iwata* [1982] (Table 1), is particularly prominent between Beni and Kusma. It contains poorly layered centimetric to decimetric subrounded pebbles of varying lithologies of Higher Himalayan and Thetysian origin. An important calcareous fraction has favored induration of the matrix. *Yamanaka and Iwata* [1982] have moreover observed some reddish brown soil on top of this level, which suggests an age probably older than 20 kyr. During reincision of this level H, numerous fill cut terraces $M_1$ to $M_5$ were formed. South of Baglung, the bottom of the paleovalley appears to be <10 m above the present river bed (Plate 3d). We infer river incision rates of at most 0.5 mm/yr. North of Beni, the bedrock beneath the H terrace fill rises up to 80 m apr suggesting a gradual upstream increase of the incision rate (Plate 3d). The terraces are not preserved north of Beni as the river valley gets steeper and narrower except near Dana (Plate 5), where two terrace treads are relatively well preserved at the confluence with the Miristi Khola and are 425 and 600 m, respectively, above the present river bed (Plates 3d and 5b). They both present a fill terrace 40 to 60 m thick, which contain poorly layered subrounded pebbles of mainly Thetysian origin and a well-indurated calcareous matrix. They might therefore correlate, one or the other, with the terrace level H of *Yamanaka and Iwata* [1982] (Plate 3d). Independent of whether we associate the upper or the lower terrace with H, we infer that the incision rate at Dana must be much larger than near Baglung.

From Dana to Lete the river flows along a steep gorge. Upstream of Lete, the Kali Gandaki valley suddenly becomes much wider and less steep (Plate 2d). The active channel is wide and braided with gravel bars covering bedrock. Preserved geomorphic features includes fluvial or fluvioglacial terraces, moraines, and lacustrine deposits with complex stratigraphic relationships are abundant [e.g., *Fort*, 1993]. A major landslide, or alternatively a glacial tongue coming from the Dhaulagiri, would have dammed the Kali Gandaki valley and induced the formation of a lake between 50-60 and 35 kyr B.P. [*Baade et al.*, 1998; *Iwata et al.*, 1982] that would have extended from Tukuche [*Fort*, 1993] to ~10 km north of Kagbeni. Upstream of Marpha, the paleolake bottom lies at or below the level of the present river. Little bedrock incision has thus occurred since ~50-60 kyr B.P. along the Tibetan reach of the Kali Gandaki.

### 3.4. Rock Uplift of the Kathmandu Basin

The Kathmandu basin is located between the Trisuli and Sun Kosi watersheds (Figure 1 and Plate 4), at an elevation of 1400 m. It lies in the wide synclonorium of the Kathmandu klippe (Figures 2 and 5). At present, the Bagmati drains the basin to the south. During the Pleistocene, however, a large lake occupied the central part of the basin. Geologic studies and drilling for aquifers indicate the existence of three stratigraphic units in the basin. The deepest and thickest unit, the Lukundol formation [*Nautiyal and Sharma*, 1961; *West and Munthe*, 1981], is characterized by fluviolacustrine facies sourced from the surrounding mountains and may reach a thickness of 500-600 m [*Yoshida and Igarashi*, 1984]. Continental vertebrate, invertebrate fossils [*Wadia*, 1951; *Gupta*, 1975] and magnetostratigraphic cross sections [*Yoshida and Igarashi*, 1984; *Yoshida and Gautam*, 1988] indicate that Lukundol sedimentation started during the middle or early Pliocene and probably ended 1.8 Myr ago. In addition, pollen assemblages suggest that vegetation at that time was similar to that encountered at present between 900 and 1800 m during the warmest periods and between 1800-3000 m during driest and cool periods. The Lukundol series are mostly undeformed, except locally south of Chapagaon (Figure 5), where the series have been tilted by 20°-25°.

These series indicate that, on the basis of paleoelevation estimates, the base of the Kathmandu basin, which presently lies at 800-900 m above sea level, might have slightly subsided since the Pleistocene. Sea level representing an absolute minimum for its initial elevation, the rock uplift rate of the Kathmandu basin ranges between –0.5 and 0.5 mm/yr.

### 3.5. Synthesis of the Terrace Record of Fluvial Incision Across the Himalayas

The terrace records along the various rivers considered in this study appear to show consistent similarities. Localized zones of intense fluvial incision are found in the Sub-Himalaya and at the front of the LH, in the Mahabarat, where the rivers are forced to cut down to compensate for active thrusting and folding. This is the case along the Bagmati across the MFT, along the Trisuli-Narayani reaches across the MFT, the MDT, and the Mahabarat, and along the reaches of the Arun River across the TKT and MFT.

In the LH, bedrock reincision has been minor since the deposition of the prominent Pleistocene fill terraces. We have obtained only poor constraints from the terrace record that indicate maximum values ranging between 0.25 and 1 mm/yr for the apparent bedrock incision rate. As discussed previously (stage 3 in Figure 3), long-term incision rates may, in fact, be higher than this apparent bedrock incision rate. However, our study of the Kathmandu basin, which is adjacent to the Trisuli River, confirms that uplift and long-term downcutting rates have been limited and probably lower than 0.5 mm/yr during the Pleistocene in the LH.

At the front of the HH the geometry of some terraces treads, and of the bedrock beneath the late Pleistocene fill, suggests that fluvial incision increases upstream along the steep gorges cut into the front of the high range. The general absence of preserved terrace levels across the high range is

**Plate 4.** Holocene and Pleistocene terraces in the Narayani watershed, along the Trisuli, Marsyandi, and Kali Gandaki (see box in Figure 1a for location). Outside our field survey extent (green brackets), terrace mapping along the Kali Gandaki and the Marsyandi has been reported from previous studies [*Yamanaka and Iwata*, 1982; *Iwata et al.*, 1982]. Along these rivers, some obvious cases of epigenetic valley, like across the moraines along the north-western branch of the Marsyandi valley have been also mapped. Note that major fill terraces are systematically observed at confluence basins [*Fort*, 1993].

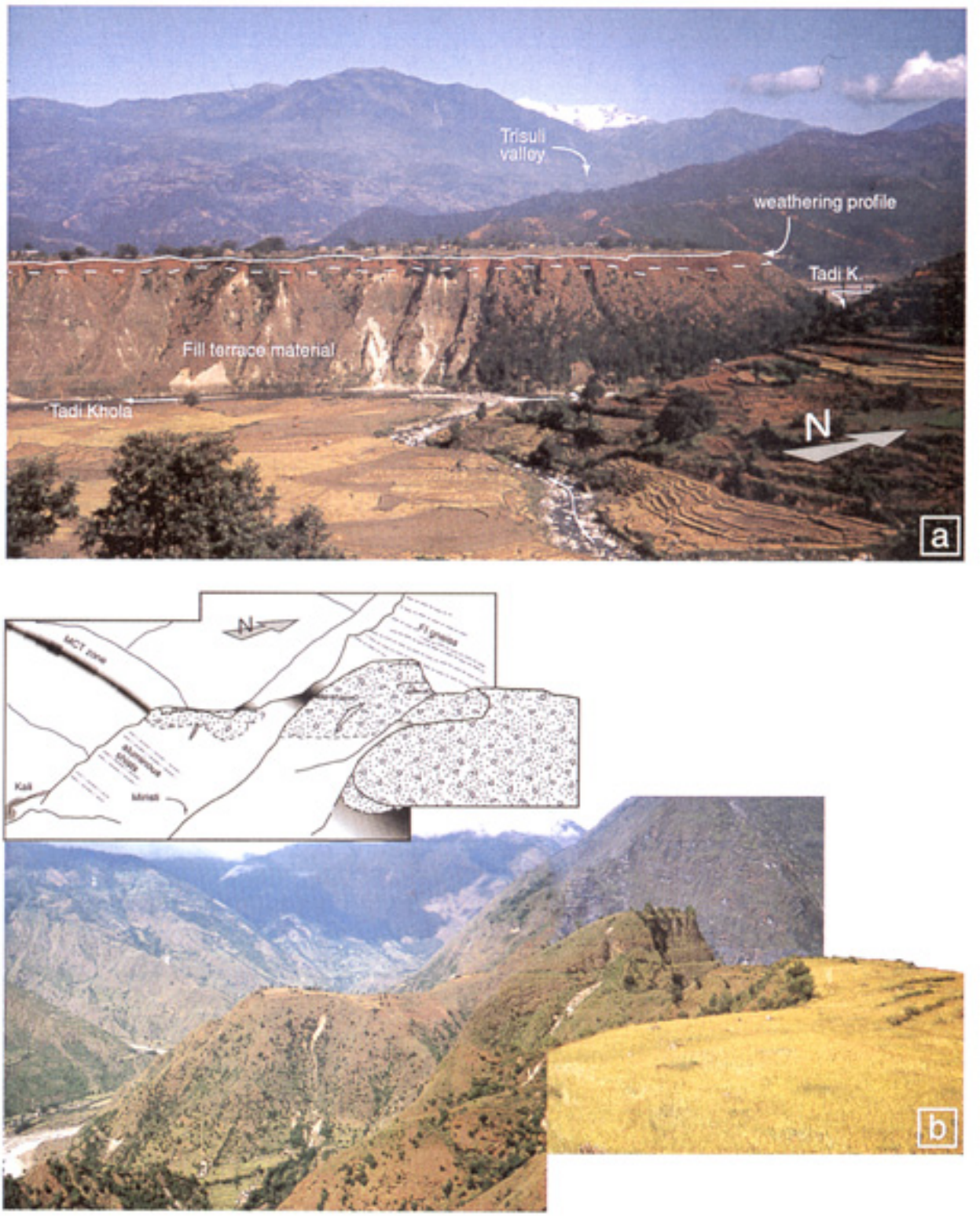


**Plate 5.** (a) Northwestward view of the Pleistocene fill terrace $Ft_1$ at the confluence between the Trisuli and Tadi Khola, south of Trisuli Bazaar. Note the 100-m-thick fill material that extends nearly down to the level of the present river bed, indicating that the river has not entrenched much deeper than the bottom of the paleovalley beneath the fill terrace. The shading in the sketch shows the 10-m-thick red weathered horizon that suggests an age probably older than 45 kyr. This outcrop is a typical example showing that little bedrock incision has taken place in the LH during the late Pleistocene. (b) (bottom) Northwestward view and (top) sketch of the 600-m-high terrace (yellow cultivated crop in the foreground and preserved promontory with layered fill deposits) and 400-m-high terrace (promontory in the background overlying the confluence with the Miristi Khola) in the Kali Gandaki gorge below the MCT zone. The bedrock crops out ~40-70 m below the terrace top.

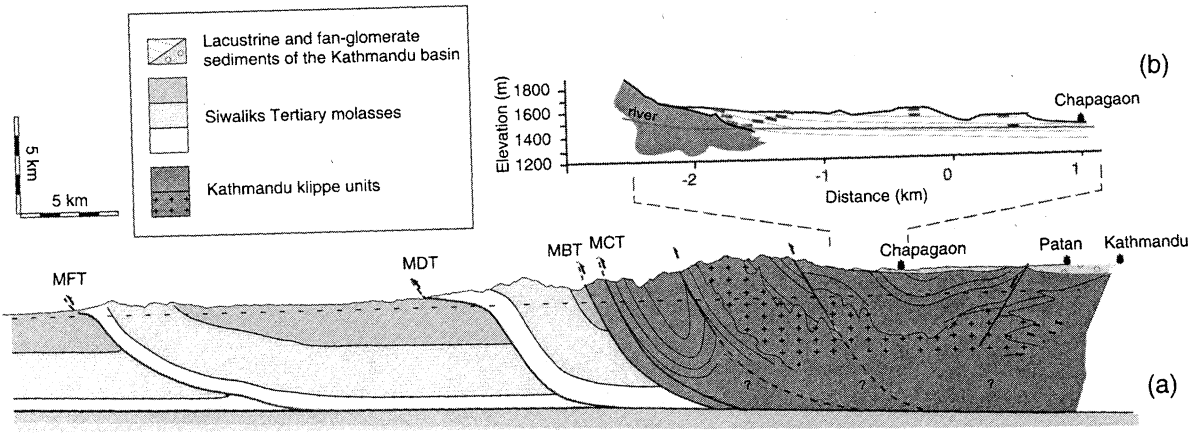


**Figure 5.** (a) Geologic cross-section of the Siwaliks along the Bakeya Khola, Mahabarat, and south part of the Kathmandu basin [*Stöcklin*, 1987; *Lavé*, 1997; *Lavé and Avouac*, 2000] (southern part of the section AA' in Figure 2). (b) Sediments of the Kathmandu basin which have not been deformed except on its southern margin, where they were northward tilted by 20°. The nearly flat decollement that extends to Patan (5 km south of Kathmandu) is inferred from balanced unfolding of the Siwaliks structures, assuming bed thickness preservation.

consistent with a particularly high incision rate there [*Merritts et al.*, 1994], as also indicated from the terraces at the confluence between the Kali Gandaki and Miristi Khola.

North of the high range, along the southern Tibetan river reaches, glacial erosion, moraines, and lakes formation have obscured the geomorphic record of river incision. However, long-term incision rates are probably much lower than in the HH. To add better constraints on incision rate in particular across the HH, we attempt in the following to develop an empirical model to estimate river erosion from the geometry of modern channels.

## 4. River Incision as Derived From the Geometry of the Modern Rivers

### 4.1. River Geometry and Bedrock Incision Rate

The geometry of a river channel expresses the river adjustment to the various external factors related to climate, lithology, and tectonics, as well as the sediment supply from surrounding hillslopes. Among other variables, the river gradient is probably the most representative of the ability of a river to transport sediments and erode the bedrock. Variation of river gradient may thus be used to detect zones of active uplift [*Seeber and Gornitz*, 1983; *Keller*, 1986]. Hereinafter we try to derive more quantitative information on incision rate from the geometry of the modern rivers within the Narayani and Sapt Kosi watersheds. We first take advantage of the dated terrace record in the Sub-Himalaya to check and calibrate a simple incison law.

Bedrock incision can result from different processes: mechanical wear by rolling and saltating bedload or by suspended load, plucking, weathering, and dissolution, or cavitation. In spite of the complexity of these various processes [e.g., *Hancock et al.*, 1998; *Sklar and Dietrich*, 1998; *Foley*, 1980a, 1980b], a simple rationale has generally been used to derive a resultant macroscopic relationship and to relate channel river properties, including stream gradient, to the rate of fluvial incision into bedrock. According to *Howard et al.* [1994] this relationship reduces to a power function of the drainage area $A$ and the local river gradient $S$,

$$i = KA^m S^n, \tag{2}$$

where $i$ is the incision rate and $K$ is an erodability coefficient depending on lithology and flow regime [*Howard et al.*, 1994; *Howard*, 1998]. So far, the above rationale neglects the fact that the abrasive capacity of a river also depends on the sediment yield [e.g., *Sheperd and Schumm*, 1974; *Foley*, 1980a, 1980b; *Sklar and Dietrich*, 1998]. This factor may possibly be a hidden parameter in the coefficient $K$ of (2), in particular, if sediment discharge or at least its abrasive effects scale roughly as a power function with upstream area [*Sklar and Dietrich*, 1998]. The physical basis for relation (2) is probably manyfold. It has been shown that different physical models in terms of either stream power, unit stream power, or fluvial shear stress can lead to (2), provided that some variables (i.e., the channel width $W$ and the discharge $Q$) obey power law scaling relationships with drainage area [*Howard et al.*, 1994; *Slingerland et al.*, 1998]. So far, field investigations are too scarce to discriminate between the various proposed models, in particular between the unit stream power and the shear stress models [*Snyder et al.*, 2000; *Stock and Montgomery*, 1999; *Howard and Kirby*, 1983]. This last relationship assumes that bedrock incision primarily relates to fluvial shear stress, which represents the force exerted by the flowing water on the underlying bedrock, defined as

$$\tau = \rho g R S_e, \tag{3}$$

where $\rho$ is the fluid density, $S_e$ is the energy slope, and $R$ is the hydraulic radius, which can be expressed as a function of the channel width and water depth $h$ in the approximation of a rectangular cross section:

$$R = \frac{2Wh}{(W + 2h)}. \tag{4}$$

The water depth can be expressed as a function of the water discharge $Q$ and $W$, provided that $U$, the depth-averaged velocity, can be estimated through mass conservation and, for example, Manning's equation

$$U = \frac{Q}{Wh} = \frac{1}{N} R^{2/3} S_e^{1/2}, \tag{5}$$

where $N \propto D_{90}^{1/6}$ is the roughness coefficient [e.g., *Chang*, 1988] and $D_{90}$ is the grain diameter not exceeded by 90% of the bed load. Below, we will assume that the roughness mainly depends on gravel size because we observed that Himalayan rivers are most generally paved with some bed load. These rivers are moreover characterized by great seasonal hydrological variations so that flow velocity and shear stress must be estimated for peak flow conditions.

In our study, as detailed below, we have estimated the slope and width of the river channel from topographic maps, digital elevation models (DEM), air photographs, and satellite images and the flood discharge from stream gauge measurements. Instead of assuming power law scaling relationships with the drainage area and using (2), we therefore prefer to allow an explicit account for these variables in computing and evaluating stream power or fluvial shear stress models.

### 4.2. Estimating River Gradient, Channel Width, and Water Discharge

In the Siwalik Hills along the Bagmati and Bakeya Rivers, river gradients were measured on a 20-m DEM derived from a stereopair of panchromatic SPOT images and from altimeter and GPS measurements [*Lavé and Avouac*, 2000]. Along the trans-Himalayan rivers within Nepal, we have measured stream gradient on 1:63,000 maps, on which elevation contour lines are spaced every 30.5 m. In Tibet, we have used a DEM [*Fielding et al.*, 1994] with a 90 m spatial resolution and derive channel profiles after elimination of local sinks.

The channel width along the various rivers was measured with an accuracy of 10-20 m from satellite images or from aerial photographs. This measurement is unambiguous most of the time because even in periods of low water level, the width of the channel during peak flow is well defined from the bare gravel and sand bars. Where width could not be measured because we did not have satellite images or aerial photograps, we estimated the width from the scaling law $W \propto Q^{0.5}$. Such a relationship is generally observed for alluvial rivers [*Leopold and Miller*, 1956; *Leopold*, 1994] and was found to be roughly consistent with our data set. However, this crude estimate was used only for the Buri, Sun Kosi, and Trisuli Rivers along their upper reaches that account for <13% of the total river length. River gradient and width measurements were then smoothed using a sliding window with a size depending on the spatial resolution on slope measurements, i.e., 200 m along the Bakeya and Bagmati Rivers across the Siwalik Hills and 1 km along trans-Himalayan rivers.

On the southern flank of the Himalayas, annual precipitation ranges between 2000 and 5000 mm (Figure 6). The rain shadow effect of the HH is such that, in south Tibet, annual precipitation drops to 100-400 mm. The Department of Hydrology of Nepal has been monitoring stream and rain gages for around 10 to 40 years [*HMG of Nepal*, 1995a,

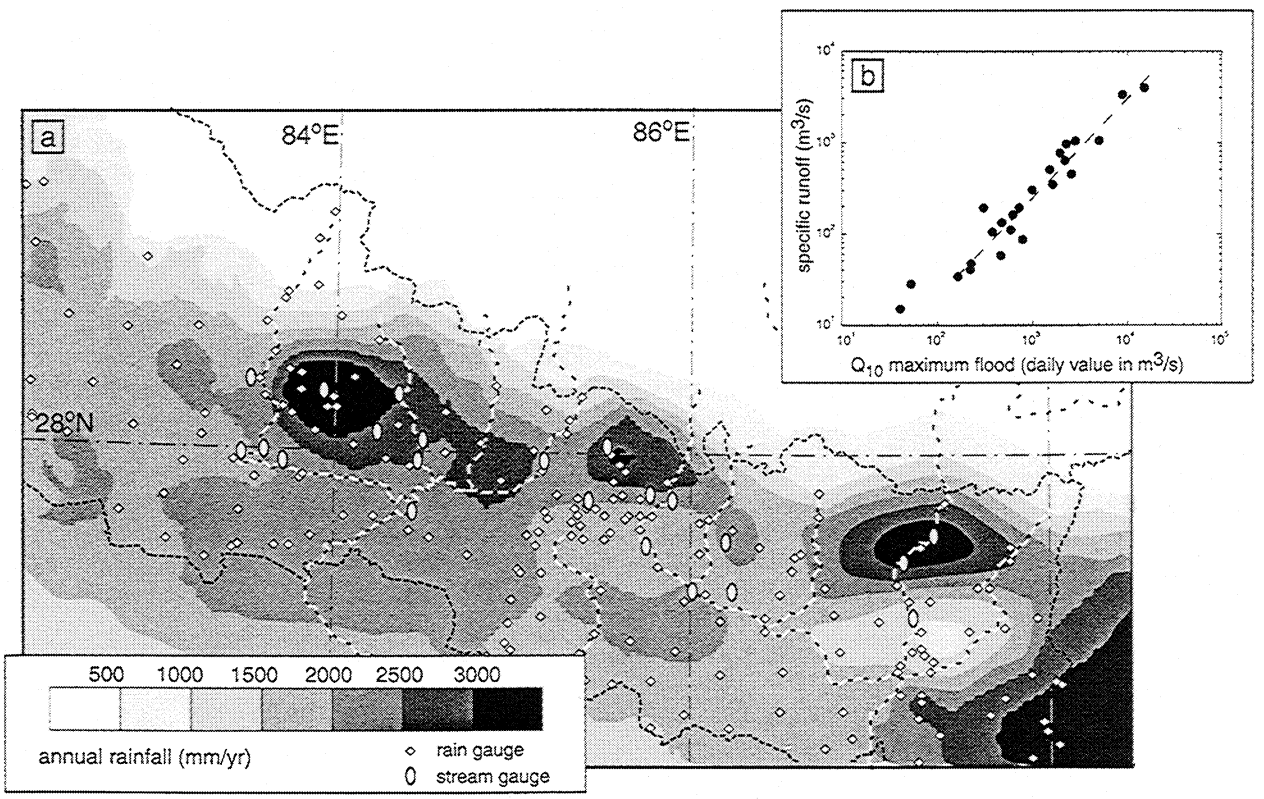


**Figure 6.** (a) Map of annual rainfall in the study area derived from 4-year record of rain gauges (white diamonds). Rivers used in this study are shown by white dashed lines. (b) Comparison of measured water discharge (10-year return maximum daily discharge) [*His Majesty's Government (HMG) of Nepal*, 1995a, 1995b] at 24 stream gauges (indicated by white elliptical dots in Figure 6a) with that computed from the precipitation map.

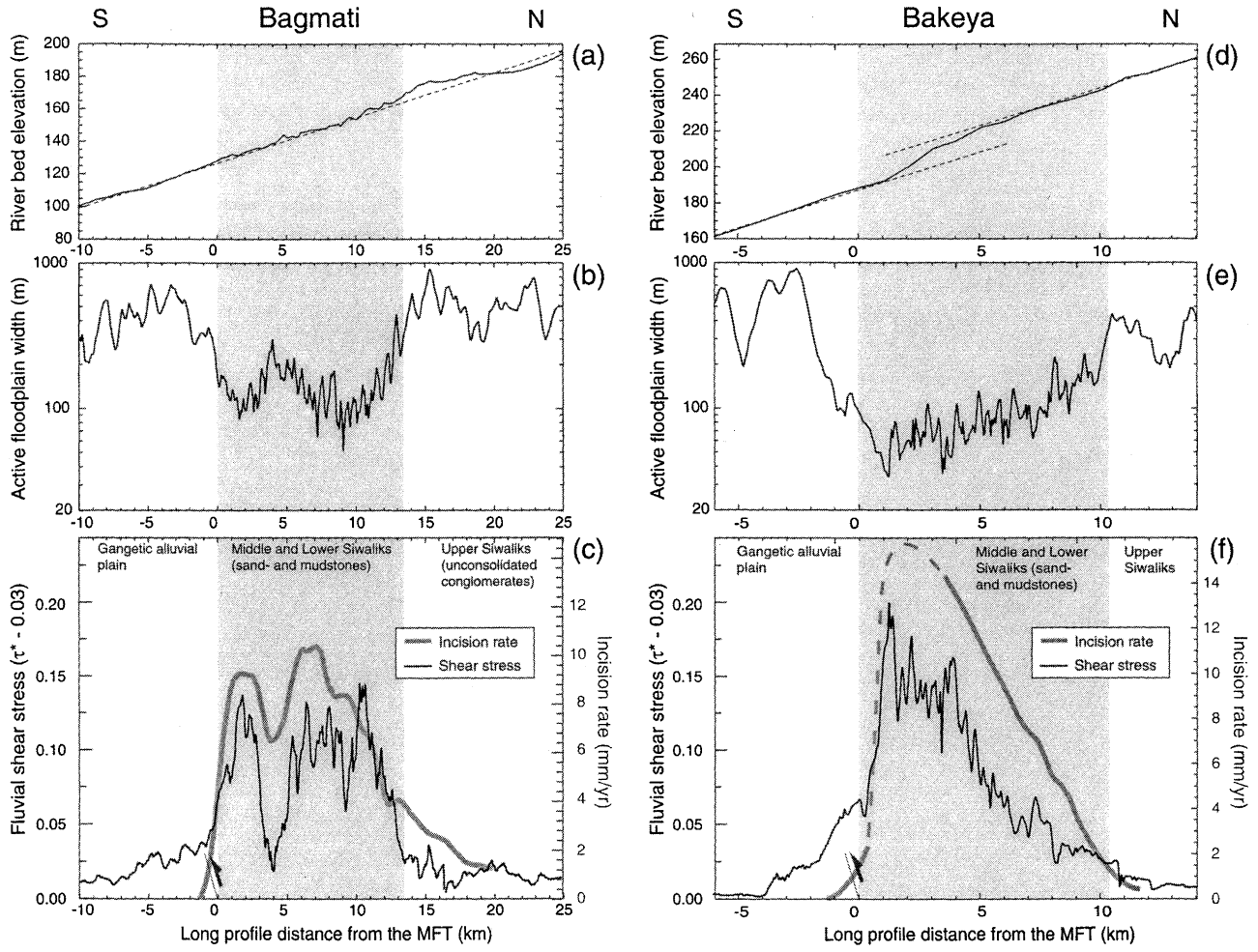


**Figure 7.** Variation of the residual Shields stress ($\tau^*$ - 0.03) (thin solid line) and of incision rate (thick shaded line) along (c) the Bagmati and (f) Bakeya Rivers. Incision rate is derived from the Holocene strath surfaces and theoretical uplift rate is derived from fault-bend folding (dashed line) [*Lavé and Avouac*, 2000] (see also Figure 4). Shields stress $\tau^*$ was derived from (b) and (e) channel width and (a) and (c) stream gradient, as described in text. Along the two profiles, discharge and pebble size were assumed constant: $Q_{10}$ = 2000 m$^3$/s and $D_{50}$ = 55 mm for the Bagmati River and $Q_{10}$ = 350 m$^3$/s and $D_{50}$ = 40 mm for the Bakeya River. Along their course, both rivers present two different behaviors when they drain noncohesive material or when they cross cohesive sandstone (light shading). Note that pebble size has been adjusted in the Gangetic plain in order for the Shields stress $\tau^*$ to be roughly 1.4 times the critical Shields stress $\tau^*_c$ = 0.03, assuming that rivers have developed stable self-formed channel width [*Parker*, 1978].

1995b]. These data indicate that the 10-year peak flow discharge follows a power law function of the drained area [*Lavé*, 1997]:

$$Q_{10} = k\overline{P}A^{0.89}, \quad (6)$$

where $\overline{P}$ is the mean annual precipitation over the catchment (Figure 6). The exponent is close to the value of 0.85 determined for the Kali Gandaki alone [*Mezaki and Yabiku*, 1984].

At each point along a river profile the drainage area and the 10-year daily peak discharge has been computed from the 30 arc sec DEM and the precipitation map (Figure 6). According to *Lavé* [1997] the decadal peak flow would correspond to the most efficient flood in carrying bed load and possibly in promoting mechanical bedrock erosion. Finally, the depth-averaged peak flow velocity $U$ is obtained numerically using a one-dimensional finite difference scheme in steady regime but accounting for width and slope variations, as well as for sinuosity [*Chang*, 1988, pp. 56-59, 212]. At this stage we can derive stream power and fluvial shear stress along the river profile from (3) to (5). This numerical approach was used only for Bagmati and Bakeya Rivers, where the spatial resolution on slope and width makes it worthwhile. Elsewhere, we simply compute flow velocity from (5) assuming that slope energy $S_e$ may be approximated from $S$, the slope of the channel bottom.

### 4.3. Calibration of an Empirical Relation in the Sub-Himalaya

In order to test and calibrate a model of river incision, we first focus on the Sub-Himalayan reaches along the Bagmati and Bakeya Rivers. These reaches cut into relatively homogeneous lithology, the lower and middle Siwalik sandstones. Moreover, the pattern of river incision is well

constrained from abundant dated Holocene terraces [*Lavé and Avouac*, 2000; *Lavé*, 1997].

Along the Bagmati, the width of the channel (Figure 7b) varies inversely with the incision rate as derived from the Holocene terraces across the rising anticline of the MFT (Figure 7c). This pattern suggests that the Bagmati River, which is characterized by a relatively large peak discharge of $Q_{10}$ = 2000 m$^3$/s, adjusts its width rather than its gradient to incise at the rate imposed by tectonic uplift. The Bakeya River, which is characterized by a smaller discharge of $Q_{10}$ = 350 m$^3$/s at the outlet in the Gangetic plain, has adjusted both variables to tectonic uplift. As along the Bagmati, the width of the channel regularly decreases with increasing uplift rate (Figure 7e), but the river profile also shows a knickpoint with a steeper gradient where the incision rate is highest (Figures 7d and 7f). It can be noted that the total stream power, which does not depend on channel width, cannot account for these width adjustments to varying incision rates, in contrast to the unit stream power or the shear stress.

For both profiles the computed fluvial shear stress actually varies consistently with river incision rate (Figures 7c and 7f), and correlates better to incision rate than to unit stream power [*Lavé*, 1997]. In addition, the erodability coefficients $K$ were found to be similar for both rivers when shear stress was normalized by the mean gravel size on the streambed (Figure 8) [*Lavé*, 1997], i.e., replaced by its nondimensional form, the Shields stress $\tau^*$:

$$\tau^* = \tau/(\rho_S - \rho)gD_{50}\,, \tag{7}$$

where $\rho$ and $\rho_S$ are the water and gravel density, respectively, $D_{50}$ is the grain diameter not exceeded by 50% (in weight) of the bed load. We estimated the value of $D_{50}$ by assuming that rivers reach an equilibrium or self-formed stable geometry [*Parker*, 1978] in the deposition plain of the Terai. It implies a constant Shields stress proportional to the critical Shields stress $\tau^*_c$ [*Parker*, 1978; *Ikeda et al.*, 1988; *Paola and Mohrig*, 1996]:

$$\tau^* \cong 1.4\tau^*_c\,, \tag{8}$$

where $\tau^*_c$ represents the threshold value for incipient motion [e.g. *Chang*, 1988]. Along the first kilometers downstream of the outlet, where slope and width are observed as roughly uniform (Figure 7), we have computed an average shear stress $\tau$ from width, slope, and discharge estimates and thus derived

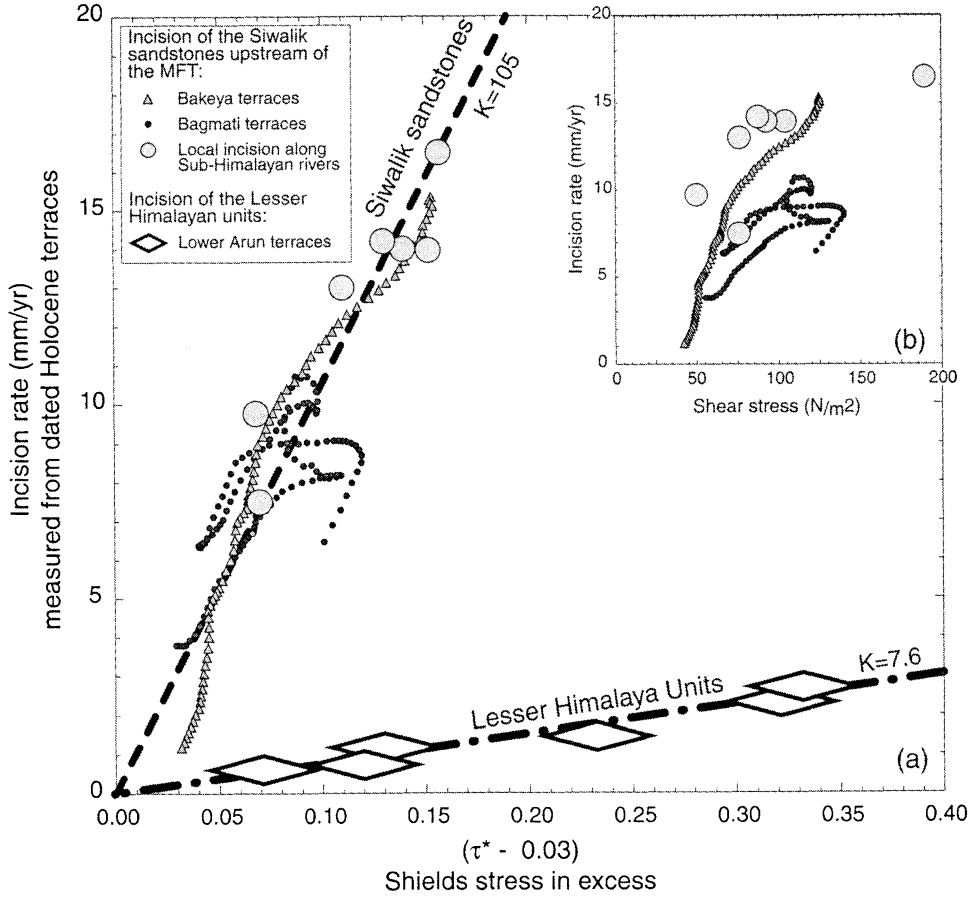


**Figure 8.** (a) Shields stress as a function of incision rate along the Bagmati and Bakeya Rivers where they cross the uplifted Siwalik sandstones at the MFT. Some points obtained from dated isolated strath terrace along other rivers in the Sub-Himalaya have been also added [*Lavé*, 1997]. These data suggest a linear relationship in the form of relation (9). The easily erodible sandstone of the Siwalik Hills is characterized by a coefficient $K$ = 105 mm/yr. The dated strath level cut in the LH schists along the Arun River (MACH5 in Plate 3a) suggests that the schists in the LH are much more resistant ($K$ = 7.6 mm/yr) than the Siwalik units. (b) Shear stress as a function of incision rate along Sub-Himalayan rivers. Data do not fit a single linear trend as observed after normalization by the median gravel size.

the median gravel size according to (7) and (8). We thus use this gravel size value to compute Shields stress across the Siwaliks, assuming that gravel size is roughly uniform all along the 20-35 km long reaches studied here. This inference derives from the observation that in the gorge and upstream, there is no long-term sedimentation and thus no fining by selective transport.

When the computed Shields stress is plotted as a function of river incision rate, as determined from the terrace record (Figure 8), the two sets of data fall along a single linear relationship. Also included in Figure 8 are a few points obtained from several dated strath terraces along other rivers crossing the sandstone units of the frontal Siwaliks belt in central Nepal [*Lavé*, 1997] (the calibration points are indicated by ovals in Figure 1a). This observation shows that the basal shear stress does indeed correlate with incision rate and that the normalizing factor in the computation of the Shields stress is adequate to yield a general relationship that does not depend on the characteristics of the watershed. The empirical relationship derived from our data can be written

$$i = K(\tau^* - \tau_b^*), \tag{9}$$

where the intercept $\tau^*_b \cong 0.03$ may be seen as a critical Shields stress. This expression implies that mechanical erosion of the strath, as proposed by *Howard et al.* [1994], requires a Shields stress $\tau^*$ in excess of some threshold value. This threshold is close to critical values for incipient motion, which have been found to range between 0.03 and 0.08 [e.g., *Buffington and Montgomery*, 1997], and might suggest that incipient motion is required before any mechanical erosion. In (9) the coefficient $K = 105$ mm/yr primarily reflects the erodability of the sandstone units of the frontal Siwaliks and the flow regime. Hereinafter we assume that the Shields stress model may also be used as a proxy for fluvial incision rate along the trans-Himalayan rivers, provided that the erodability coefficient may change according to the incised lithology.

### 4.4. Application to the Rivers Crossing the Entire Range

**4.4.1. Lithologic calibration.** Plate 6 shows how river width, gradient, and water discharge vary along the trans-Himalayan rivers in the study area. It should be noticed that the rivers have different width and slope profiles that probably relate to their different geological setting and hydrological characteristics (size of watershed, position with respect to rainfall, etc). They all show channel narrowing and knickpoints that roughly coincide with the front of the HH. The comparison with the knickpoint along the Bakeya River suggests that in the upper reaches, where the rivers flow along narrow gorges, the steeper gradients might actually reflect an increase in fluvial incision rate. These rivers cut across different lithologies so that part of the observed variations might reflect erodability contrasts rather than variations in incision rates, as observed elsewhere [*Stock and Montgomery*, 1999].

We have therefore tried to calibrate (9) for lithologies other than the moderately indurated Siwalik sandstone. We distinguish between the metasediments of the LH and the crystalline units of the HH.

Incision rates of the Arun River into the metasediments and orthogneisses of the LH (section 3.3.1) indicate that these units are far less erodible than the Siwalik sandstones and may be characterized by a value of $K = 7.6$ mm/yr (Figure 8). This calibration implies a variation of the incision rate derived from the Shields stress that matches the pattern defined by the elevation of the $T_0$ strath above the present river bed (inset in Figure 9a). The presumed early Holocene strath terraces along the Trisuli River also corroborates this calibration (inset in Figure 9b).

LH series are mostly quartzite, schist, sandstones, orthogneiss, marble and limestones. Pebble abrasion studies [*Krumbein*, 1941; *Kuenen*, 1956] indicate that these different rocks may have distinct erodibilities. However, because of the lack of more constraining data and precise geologic maps we assume a uniform erodability. Rock types of the Thetysian series present some similarities with those of the LH; we therefore assume they have the same erodability coefficient $K = 7.6$ mm/yr.

In the absence of dated strath surfaces cut into the crystalline units of the HH, we could not calibrate our law directly for this lithology. However, we have computed the shear stress on both sides of the MCT along 5-10 km long reaches for more than 30 major and minor rivers. Since the contact between the units of the HH and LH is not always exactly at the front of the HH but may also follow the contour of the Kathmandu klippe, the observed shear stress discontinuities are probably due to lithological contrasts rather than to differential uplift. We have found that setting a value of $K_{HH} = 0.8K_{LH}$ for the HH units compensates for the systematic change of Shields stress at crossing of the MCT.

**4.4.2. Pebble size estimation.** Along the short reaches of rivers crossing the frontal Siwaliks Hills, pebble size may be considered uniform. In contrast, along the trans-Himalayan rivers, mean pebble size evolves significantly. Numerous pebble size measurements have been made along the Kali Gandaki by *Mezaki and Yabiku* [1984], and they show a clear decrease of the mean and maximum size from $D_{50} = 70$ mm and $D_{90} = 600$ mm in the Higher Himalayan gorges down to $D_{50} = 45$ mm and $D_{90} = 110$ mm at the outlet in the Gangetic plain. This pebble size downstream decrease [*Mezaki and Yabiku*, 1984] may be approximated according to

$$D_{50} = k_{50}A^{-0.1}, \tag{10}$$

$$D_{90} = k_{90}A^{-0.2}. \tag{11}$$

The negative exponent reflects downstream fining, probably due to abrasion. These power laws lead to limited variations (<40%) along the trans-Himalayan rivers, so that they have a limited effect on along-stream variation of the Shields stress. However, we consider large uncertainties for gravel size into the error bar computation (see Appendix A).

**4.4.3. Incision profiles and comparison with terrace records.** Using these calibrations, we are then able to derive incision rates along all the trans-Himalayan rivers in the study area (Figure 9), including an estimate of error bars (Appendix A). Obviously, the calibrations only account for the lithology variations at large scale. There are strong local lithological variations within the LH or HH units that are not accounted for. The lithology is thus probably the main source of variability in the computed incision rates. In spite of these short- scale variations all the profiles appear to yield a consistent pattern (Plate 7). It thus appears that owing to their different hydrological and geological setting, the various rivers display slightly different geometries, but they all yield about the same incision pattern with incision rates of the order

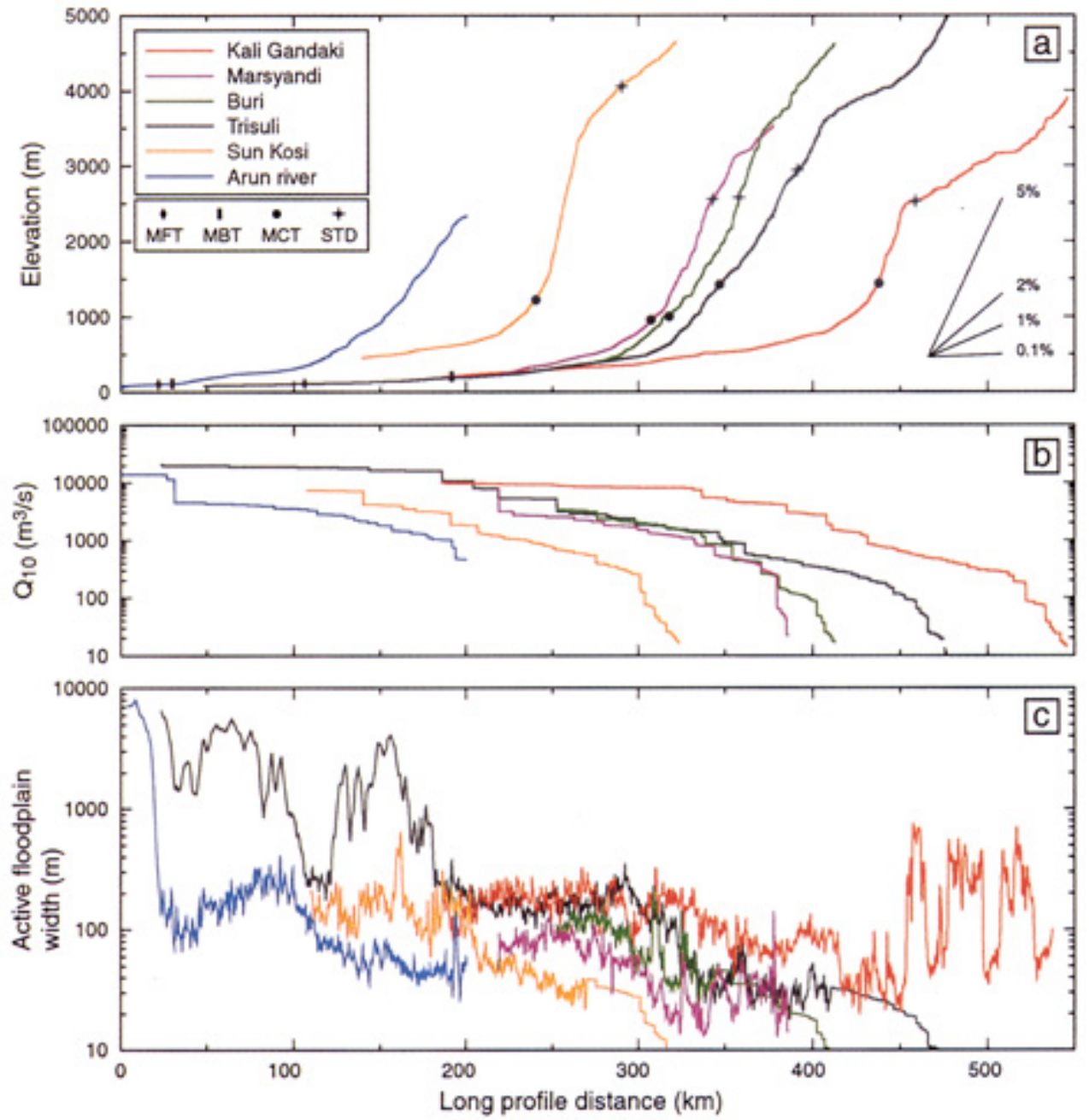


**Plate 6.** (a) Elevation, (b) 10 years flood discharge, and (c) width of the modern channel along the studied trans-Himalayan rivers, the Arun, Trisuli, Kali Gandaki, Marsyandi, Buri, and Sun Kosi. Major structural contacts are shown along each elevation profile with different symbols.

of 0.5 to 2 mm/yr in the LH and between 4 and 9 mm/yr over a distance of ~50 km in the high range. Incision rates are poorly constrained in southern Tibet but seem relatively small (<1 mm/yr). The most striking feature appears at the transition between the LH and the HH, where the warping of the terraces also suggests differential uplift. A more general comparison with the terrace record also evidences in the LH a systematic bias between calculated incision rate (between 0.5 and 2 mm/yr) and the maximum rate derived from the terrace study (<0.5 mm/yr) (Plate 7). As discussed in section 3.5 and Figure 3, this bias might arise from the systematic difference between the bedrock incision rate $i_b$, as derived from the Shields stress computation, and the long-term downcutting rate $i_{LT}$ estimated from the terrace study.

We may also compute the amount of material eroded away from a section of the range by integrating the incision profiles of Plate 7. We obtain consistent values for all trans-Himalayan rivers of around 315 km$^2$/Myr when the contribution of the material eroded from the Siwalik Hills is neglected and 375 km$^2$/Myr otherwise (Table 2). The consistency in form, amplitude, and integral between the incision profiles obtained along the various rivers suggests that Shields stress approach provide also a useful estimate for fluvial erosion along the trans-Himalayan rivers.

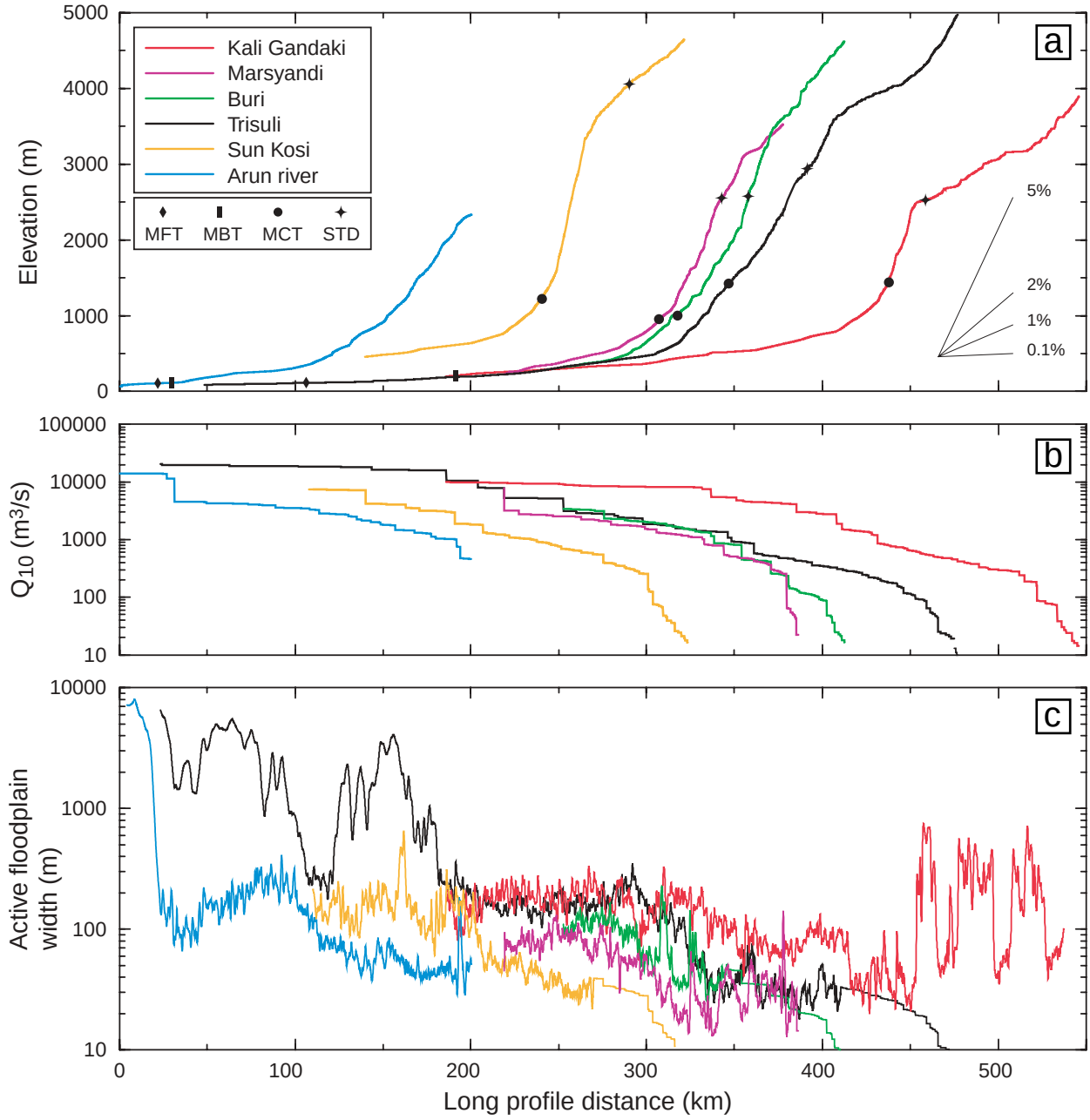
a
b
c
Kali Gandaki
Marsyandi
Buri
Trisuli
Sun Kosi
Arun river
MFT
MBT
MCT
STD
5%
2%
1%
0.1%
Elevation (m)
$Q_{10}$ ($m^3/s$)
Active floodplain width (m)
Long profile distance (km)
0
1000
2000
3000
4000
5000
10
100
1000
10000
100000
0
100
200
300
400
500

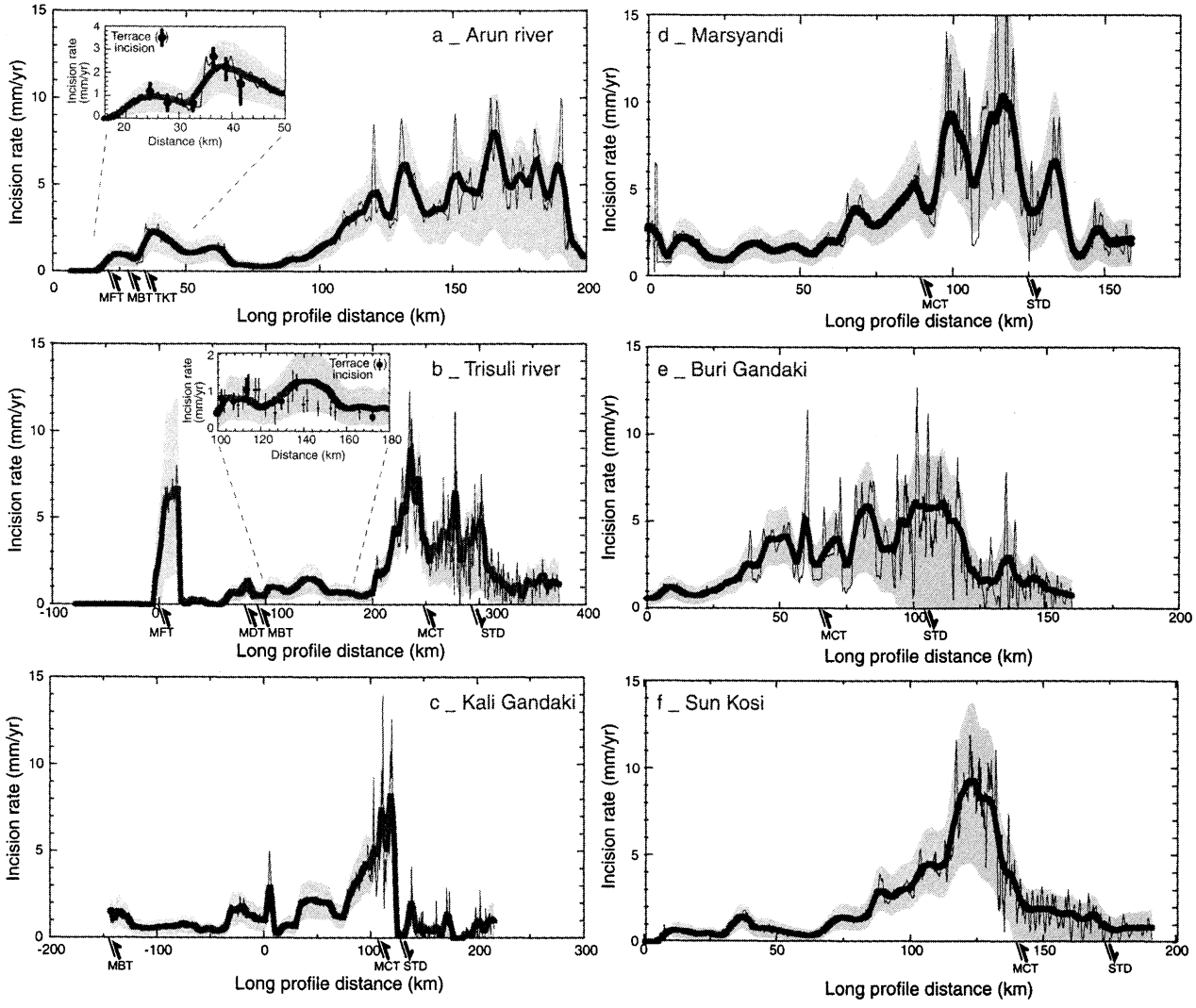


**Figure 9.** Incision rate profiles along (a) Arun, (b) Trisuli-Narayani, (c) Kali Gandaki, (d) Marsyandi, (e) Buri, and (f) Sun Kosi Rivers. Thick line was obtained by averaging over a 10-km-wide sliding window in order to filter out the variability of incision rates at small scale (thin solid line). The shaded area shows the confidence domain on incision rates. Major structural contacts are shown along the distance axis of each profile. Inset in Figure 9a shows the incision rates derived at a few sites where the Arun River has cut an early Holocene (9.1 kyr cal. B.P.) strath in the metasediments of the LH. Inset in Figure 9b shows the incision rates derived from narrow strath between Simpani and the confluence with the Seti Khola (thick symbol is elevation measured with an altimeter; thin symbol is estimated elevation on the bank opposite to the road). These straths are assumed to be early Holocene in age by analogy with the major Holocene strath levels in the Sub-Himalaya and Lesser Himalaya.

## 5. Fluvial Incision and Landscape Denudation

In the HH of northern Pakistan, it has been shown that hillslopes are near their critical slopes for mass movement, so that the topography evolves by landslides and rockfalls at the rate imposed by fluvial incision [*Burbank et al.*, 1996]. On a different context, *Hovius et al.* [1997] have shown that landslides account for nearly all sediment production along the active front of the Southern Alps in New Zealand. Even in tectonically less active setting, the critical failure angle seems to limit slopes and relief [*Schmidt and Montgomery*, 1995]. Bedrock landsliding driven by fluvial incision is also probably the dominant factor in the Himalayas of Nepal, especially in the high range, where the steep hillslopes often bear evidence of recent landsliding. In the following, we attempt more particularly to test the view that fluvial downcutting in the High Range would be the rate-limiting process that drives hillslope processes, so that denudation should equal fluvial incision.

Because the projected fluvial incision profiles (Plate 7) are fairly similar in shape and integral value, we may assume a cylindrical model of denudation that matches the average fluvial incision profile (Figure 10a) and, in the LH, the terrace incision rates. Along the fluvial network, we thus compute sediment yield assuming that denudation rate keeps pace with fluvial downcutting, and we compare these synthetic values to field measurements of suspended load for 11 catchments

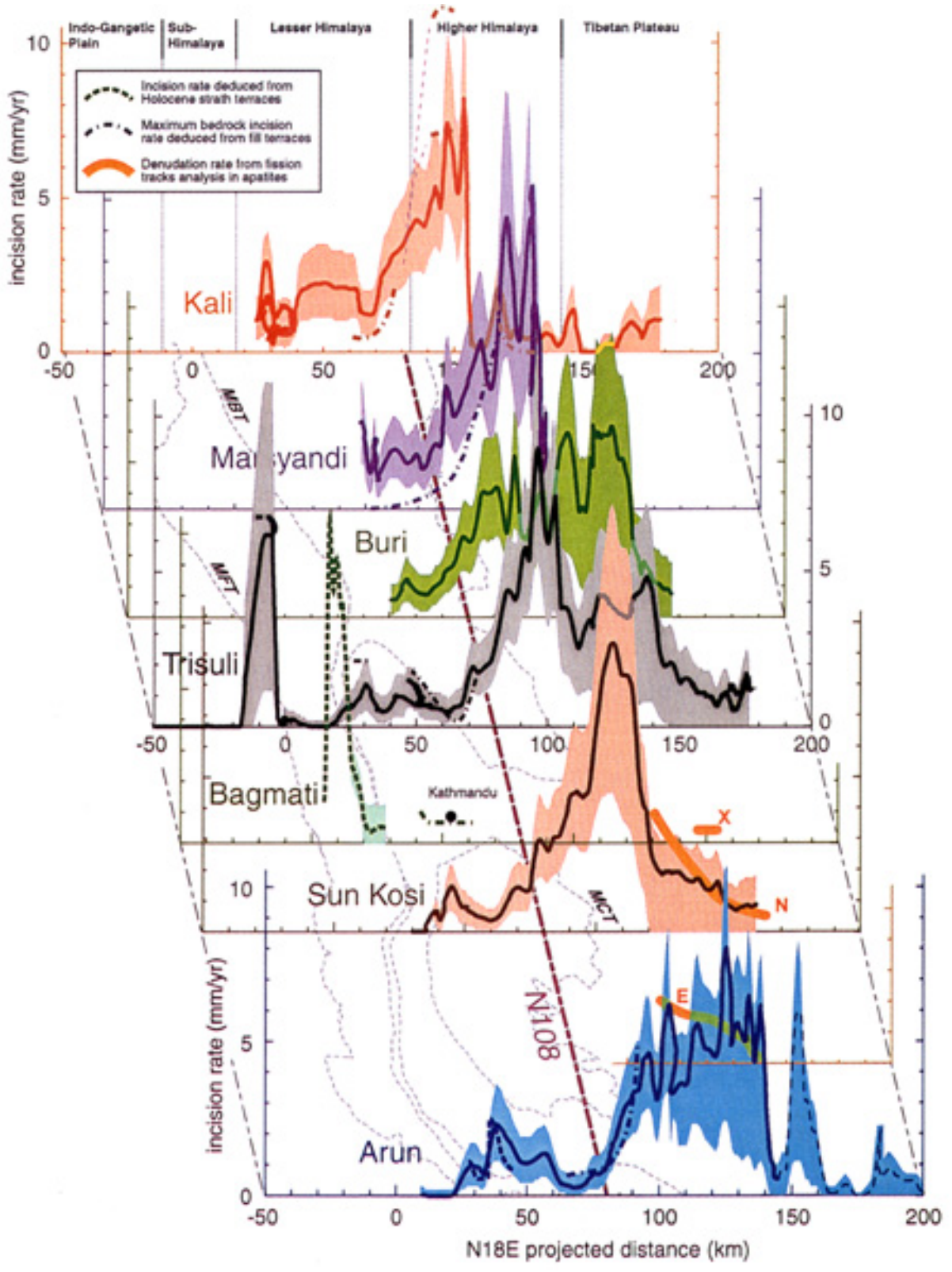


**Plate 7.** Synthesis of incision profiles derived from the terrace records and Shields stress along the studied rivers. All the profiles indicate a subdued rate of incision in the LH (0.5-2 mm/yr), which increases abruptly at the front of the HH, marked by the N108°E trending line. Incision rates are poorly constrained but seem lower along the south Tibetan reaches, in agreement with low values of the denudation rates derived from fission track (orange profiles) north of Xixapangma (X) [*Searle et al.*, 1997], north of Nyalam (N) [*Yanbin and Jun*, 1998], and south of the mount Everest (E) [*Bergman*, 1993]. Note that a rough estimation of the incision profile, derived from GTOPO30, the 30 arc sec U.S. Geological Survey DEM, was also added for the upper Arun River (blue dashed line).

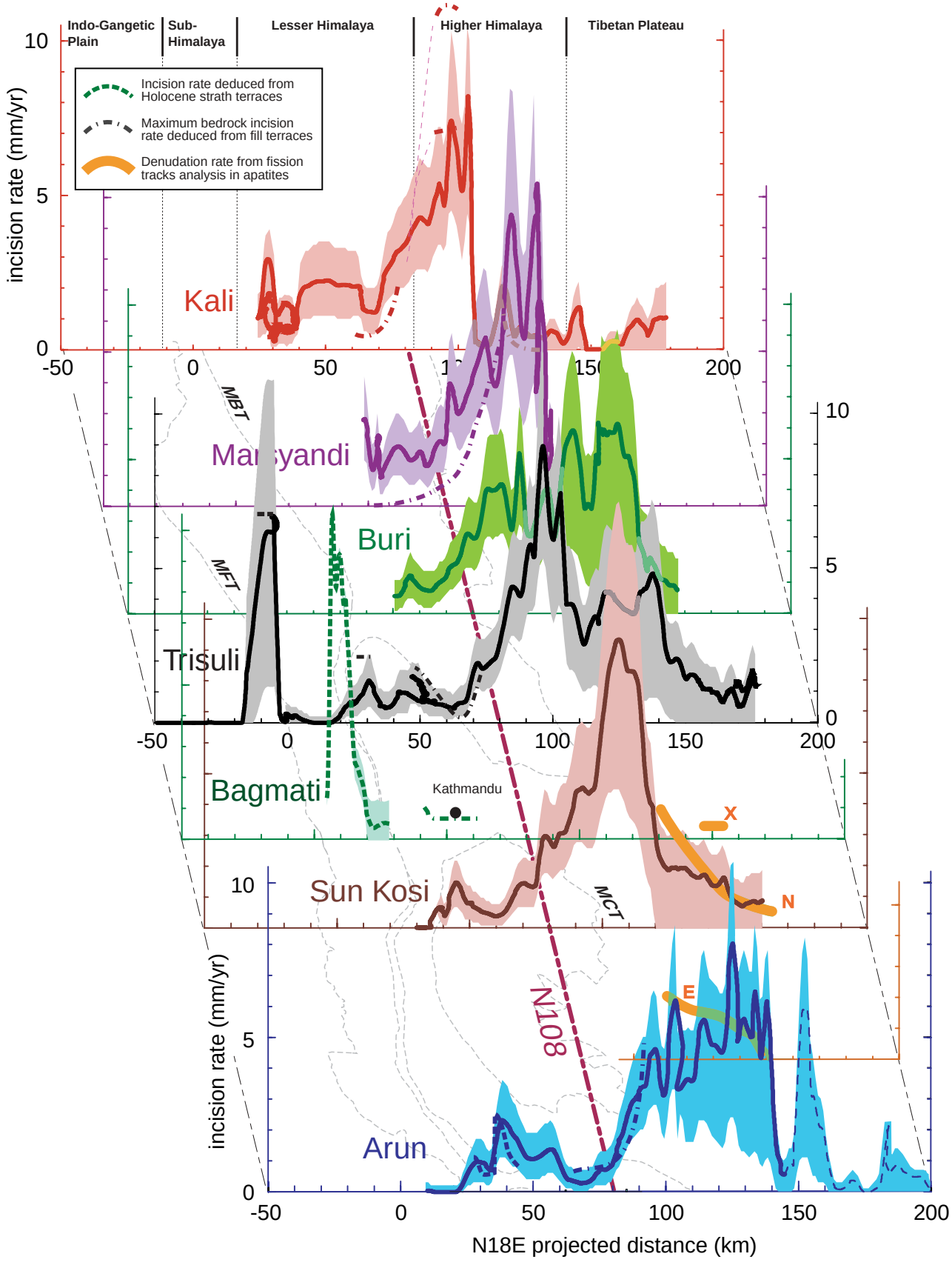
Indo-Gangetic Plain
Sub-Himalaya
Lesser Himalaya
Higher Himalaya
Tibetan Plateau
Incision rate deduced from Holocene strath terraces
Maximum bedrock incision rate deduced from fill terraces
Denudation rate from fission tracks analysis in apatites
incision rate (mm/yr)
Kali
Marsyandi
Buri
Trisuli
Bagmati
Kathmandu
Sun Kosi
Arun
MBT
MFT
MCT
N108
X
N
E
N18E projected distance (km)

**Table 2.** Denudation Rates Along Profiles Transverse to the Range Obtained by Integrating (After Projection Onto a Plane Perpendicular to the N108°E Strike of the Range) the Incision Rates Along the Different Trans-Himalayan Rivers[a]

| River | Denudation Rate Upstream of the MBT, km$^2$/Myr | Denudation Rate Upstream of the MFT[b], km$^2$/Myr |
|---|---|---|
| Kali Gandaki | 275 +140/-145 | 345[c] |
| Marsyandi | 260 +135/-125 | >330[c] |
| Buri Gandaki | 320 +160/-220 | 390[c] |
| Trisuli and Narayani | 355 +180/-210 | 415 +250/-250 |
| Sun Kosi | 330 +170/-195 | 400[c] |
| Arun and Sapt Kosi | 360 +200/-220 | 370 +205/-225 |

[a]This computation assumes denudation rates at pace with fluvial erosion. The contribution of the Siwaliks in terms of eroded area was reduced by a factor 0.8 in order to account for the difference of density with respect to the LH and HH rocks. With such a correction, these integral values may be used directly for mass balance and compared to suspended load measurements. A similar correction is applied for computation presented in Figure 11.

[b]After addition of the Siwaliks contribution.

[c]Estimated contribution.

within the Narayani and Sapt Kosi watersheds (Table 3, and Figures 10b and 11).

The two estimates compare well (Figure 11) but it appears that measured suspended loads yield denudations rates that are systematically lower by ~20%, compared to those computed from fluvial incision. This may suggest that fluvial erosion proceeds more rapidly than denudation on hillslopes and that the landscape is thus not at equilibrium. There are, however, plausible explanations. First, the two estimates are associated with different time scales: River profiles represent hundred of thousands of years of geomorphic evolution, whereas suspended load measurements correspond to present-day erosion rates. The latter denudation estimate is probably sensitive to transitory phenomena like temporary sediment storage in fill terraces and moraines or, alternatively, to increasing sediment supply during reincision of these stored sediments. Second, most of the integral values depend on the calibration of the Lesser Himalayan erodability coefficient along a single reach in the Arun valley and might bias our fluvial incision model. Finally, bed load usually amounts to a significant fraction of the total sediment yield. The two estimates could be reconciled for an average fraction of 20%, which is slightly larger than the values of 10-20% that are generally admitted.

At a larger scale we may also compare denudation rates in the Himalayas of central Nepal with the amount of sediment deposited in the foreland and in the Bengal Fan. In that case we must also take into account the Sub-Himalayan contribution (Table 2) either estimated from our model of fluvial erosion, where possible, or by assuming a denudation rate at pace with tectonic uplift [*Lavé*, 1997; *Hurtrez et al.*, 1999]. The fluvial incision model predicts a sediment flux of 375 km$^3$ km$^{-1}$ Myr$^{-1}$ on average for a section perpendicular to the range. For comparison, *Métivier et al.* [1999] have calculated that $1\text{x}10^6 \pm 3\text{x}10^5$ km$^3$ of sediments were eroded away from the Himalayas and deposited in the Bengal fan and in the Gangetic basin during the last 2 Myr. The Gange and Brahmaputra drain a 1800-km-long stretch of the Himalayan arc. Volume accumulation in peripheral basins over that period corresponds therefore to 280 ± 110 km$^3$ km$^{-1}$ Myr$^{-1}$ of denudation from an average section across the range.

Despite a probable overestimation of the fluvial incision from our shear stress model, we conclude that to a first order, denudation of the whole landscape proceeds at pace with fluvial downcutting. In the high range, these results are consistent with the simple view that the topography is eroded at the rate imposed by fluvial downcutting. If landsliding is the dominant erosion process on hillslopes, as observed in other active mountains [*Hovius et al.*, 1997; *Burbank et al.*, 1996], fluvial downcutting would thus drive the landslides frequency.

In addition, it can be noted that the rate and pattern of denudation have been roughly constant since the late Pleistocene. First, the mean erosion fluxes during the Quaternary period are similar to present ones. This supports the notion that present-day sediment fluxes reflect sustained erosion rates rather than transient storage or reductions in sediment storage along Himalayan valleys (see also discussion by *Métivier and Gaudemer* [1999]). Second, in southern Tibet and the HH, landscape denudation rates as obtained from thermochronologic data, mainly apatite fission track data [*Searle et al.*, 1997; *Yanbin and Jun*, 1998; *Bergman*, 1993], display a roughly similar pattern to fluvial incision profiles (Plate 7). For an assumed thermal gradient of 30°C/km, these data indicate denudation rates between 0 and 4 mm/yr, which are consistent with our river incision rates (Plate 7).

## 6. River Incision, Uplift, and Crustal Deformation

We now investigate how river incision profiles, particularly the elevated rates across the HH, and the previous observation, that landscape denudation proceeds at pace with fluvial downcutting, might be used to assess various models of mountain building. First, we consider a geomorphic model [*Montgomery*, 1994; *Masek et al.*, 1994], and next turn to models which explicitly include the role of crustal thickening.

### 6.1. Headward Regressive Erosion and Isostatic Rebound of the Edge of the Tibetan Plateau

*Burbank* [1992] suggests that Late Cenozoic change in deposition patterns in the Gangetic plain was the expression of a major change in tectonics and erosion processes in the Himalayas. Enhanced erosion would have overcome thickening and southward propagation of the range and caused recent Himalayan peak uplift. In such a scenario, we expect that valleys deepen and river downcutting leads to intense regressive erosion into a weakly dissected topography. In this case of headward regressive erosion at a tectonically inactive edge of the Tibetan Plateau, we may follow *Montgomery*'s [1994] assumption that fluvial incision carves deep valleys without peak erosion (a necessary assumption in order for enhanced erosion to lead to relief increase and peak uplift). In that case, the mean denudation rate $e(x,t)$ would amount to half the river incision rate $i(x,t)$ over the same period:

$$e(x,t) = \frac{1}{2} i(x,t), \tag{12}$$

where $x$ is the distance perpendicular to the Himalayan arc

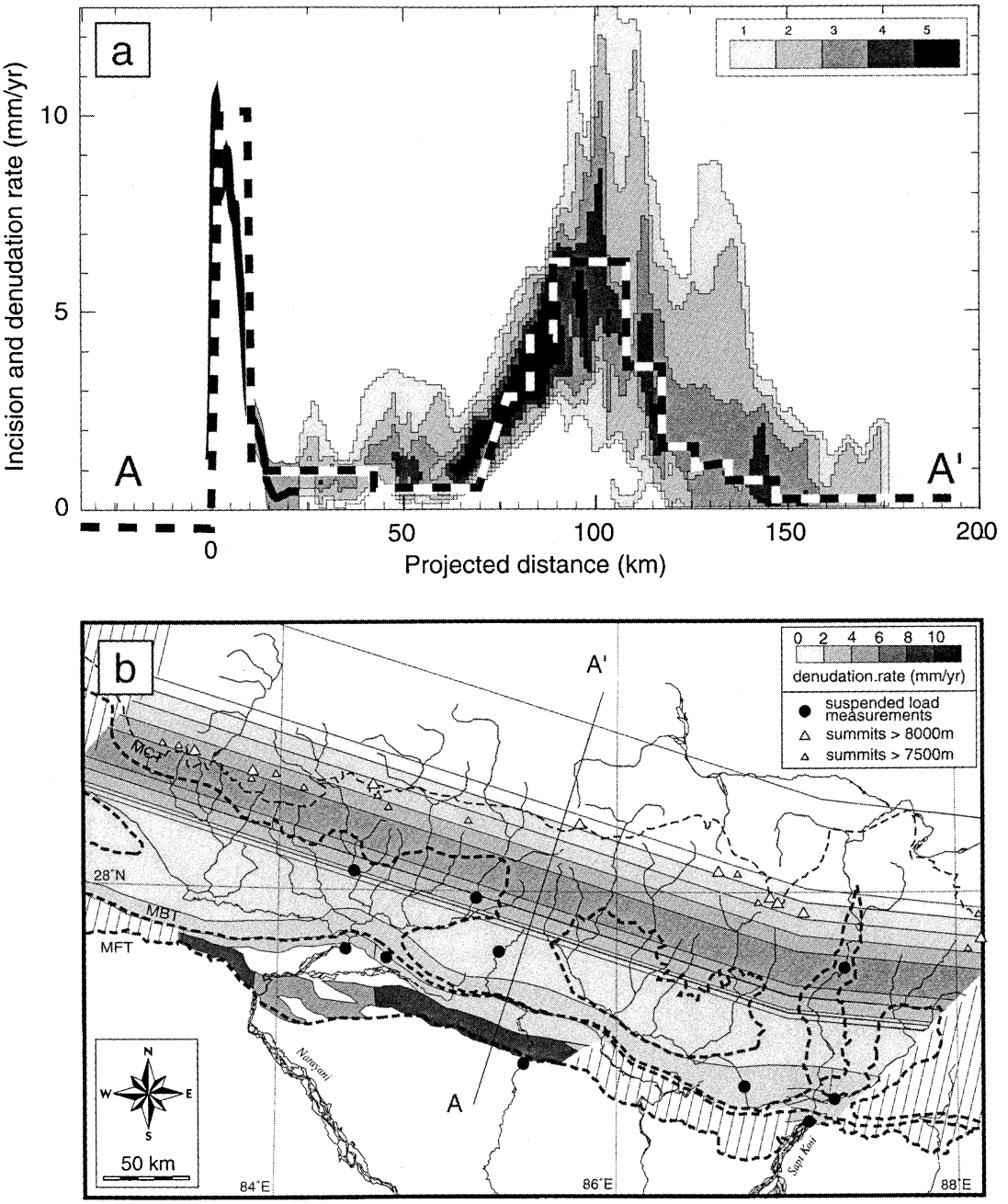


**Figure 10.** (a) Stacked incision rates, with their confidence domain, for the five rivers between the Kali Gandaki and Sun Kosi, projected onto a N18°E profile. The shading indicates overlapping confidence domains. The dashed line is a simplified 2-D model that assumes that the denudation does not vary much along strike at the scale of the study area. (b) The resulting denudation rates in mapview. A slight change in the azimuth of the model axis of symmetry at ~87°E accounts for the corresponding change in the azimuth of the front of the HH. Also shown, incision rates in the Siwaliks are interpolated from dated terraces studies and structural studies [*Lavé*, 1997; *Lavé and Avouac*, 2000], assuming steady state topography [*Hurtrez et al.*, 1999]. The locations of hydrological stations where suspended loads were measured and the corresponding catchments are also shown.

and $i(x,t)$ is counted positively in the case of net erosion. This out-of-equilibrium situation would induce wholesale landscape denudation to be 50% lower than fluvial incision along trans-Himalayan rivers. As explained in section 5, our data indicate that the difference is probably <20%.

Independently, the scenario may be constrained by investigating regressive erosion rates across the HH. To simplify, we assume that the knickpoint geometry is roughly preserved during regressive incision and propagates backward at a northward rate $m(x,t)$. This rate depends on the stream gradient at the knickpoint,

$$m(x,t) = \frac{1}{S(x)}\left[i(x,t) - v(x,t)\right], \tag{13}$$

**Table 3.** Mean Denudation Rates over 11 Catchments Within the Study Area as Estimated From Suspended Load Measurements

| River | Drainage Area, km$^2$ | Estimated Denudation Rate[a], mm/yr | References[b] |
|---|---|---|---|
| Tamur | 5770 | 2.5 ± 0.5 | 1, 2, 3 |
| Sun Kosi | 19000 | 1.4 ± 0.4 | 1, 2, 3 |
| Arun | 34000 | 0.6 ± 0.1 | 1, 2, 3 |
| Arun | 26600 | 0.4 | 5 |
| Sapt Kosi | 60000 | 1.1 ± 0.1 | 1, 4, 9 |
| Marsyandi | 2000 | 2.5 | 7 |
| Trisuli | 4100 | 0.7 | 3 |
| Narayani | 31000 | 1.3 | 8 |
| Lothar | 170 | 0.8 | 6 |
| Bagmati | 2800 | 1.1 | 9 |
| Bagmati | 250 | 0.5 ± 0.1 | 6, 9 |

[a]From suspended load measurements.

[b]References 1, 2, 3, and 4 are compilation of different sources by *Delcaillau* [1992]: 1, *Carson* [1985]; 2, *Brunsden et al.* [1981]; 3, *Laban* [1978]; 4, *Zollinger* [1979]; references 5, 6, 7, 8, and 9 are related to dam projects, courtesy of His Majesty's Government (HMG) of Nepal Undertaking, Nepal Electricity Authority: 5, *HMG of Nepal* [1991b]; 6, *HMG of Nepal* [1989]; 7, *HMG of Nepal* [1994]; 8, *HMG of Nepal* [1982]; 9, *HMG of Nepal* [1991a].

where $v(x,t)$ represents the rock uplift rate. We note that here the rivers drain perpendicular to the range, which is always the case for major rivers across the HH. We furthermore assume local isostatic compensation and obtain, according to (12) and (13),

$$m(x,t) = \frac{1}{S(x)}\left(1 - \frac{\rho_c}{2\rho_m}\right) i(x,t), \qquad (14)$$

where $\rho_c$ and $\rho_m$ are crust and mantle density, respectively. The assumption of flexural isostatic compensation would be more realistic in view of the high flexural rigidity assigned to the Indian Plate [*Lyon-Caen and Molnar*, 1983, 1985]. We have assumed local compensation for the sake of simplicity, but it should be noted that this hypothesis overestimates the isostatic rebound in the area of maximum denudation and hence leads to an underestimation of the rate of headward regressive erosion.

Given that the trans-Himalayan rivers all incise at about the same rate but have different slope profiles depending on the size and setting of their watershed, they should recede at different rates. We obtain 90-100 mm/yr for the Trisuli and Arun Rivers, 55-60 mm/yr for the Marsyandi and Kali Gandaki, and 40-45 mm/yr for the Buri Gandaki and Sun Kosi. This process would produce a festooned range front and seems irreconcilable with the linear trend of the front of the HH and with the N108°E alignment of the knickpoints along the trans-Himalayan rivers (Plate 7). In addition, the estimated rates of regressive erosion are improbably high. It would have taken less than a million years for the knickpoint along the Trisuli to move from the MFT to its present position at the plateau edge. Deposition in the Kathmandu basin, which lies 20-30 km south of the knickpoints, should postdate regressive erosion of the plateau edge and thus be younger than 0.3 and 0.7 Myr according to the knickpoint migration rate along the Trisuli and Sun Kosi Rivers, respectively. This scenario is inconsistent with the reported age ≥1.8 Myr B.P. for the Lukundol formation [e.g., *Yoshida and Gautam*, 1987]. We therefore believe that enhanced erosion in the Late Cenozoic and accompanying regressive erosion did not play a major role in the creation of knickpoints along the trans-Himalayan rivers and in peak uplift by isostatic adjustment (see also discussion by *Whipple et al.* [1999]). These geomorphic features must therefore rather result from an active tectonic control, as already proposed by *Seeber and Gornitz* [1983] and discussed in section 6.2.

### 6.2. Himalayan Thrust Geometry and Associated Uplift

**6.2.1. Past tectonics imprints.** *Harrison et al.* [1997] found evidence for recent reactivation of the MCT and suggest that the front of the high range would, in fact, reflect the late Miocene reactivation of the MCT. However, it is not clear that any event occurring in the late Miocene would be reflected in the present-day topography of the high range. At the present rates of incision (4 to 8 mm/yr), it would have taken <5 Myr to strip off 15 km of crustal material, giving plenty of opportunity for the relief to change since late Miocene.

More generally, an upper bound to the transient response time to tectonic forcing is the time needed for the trans-Himalayan rivers to reach their equilibrium profile and for their upstream part to reach their present elevation, when starting from a nearly horizontal channel. It follows that

$$\Delta t_{response} \leq \Delta H / v \cong 0.8\,\text{Myr}, \qquad (15)$$

if we assume an average $v$ = 5 mm/yr incision rate in the High Range and a maximum topographic step at the knickpoint

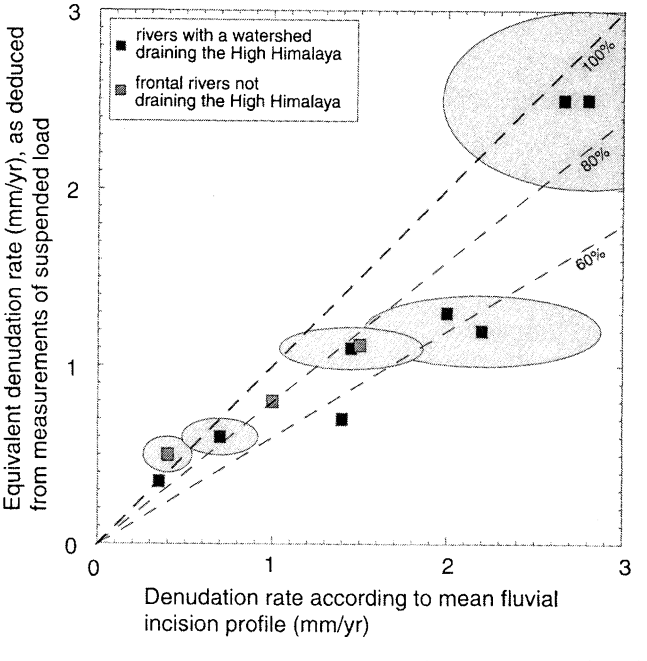


**Figure 11.** Comparison between denudation rates predicted by the denudation model in Figure 10b and the denudation rates inferred from the suspended loads measured at the stations indicated in Figure 10b. See values in Table 2. For some stations, an error bar (shaded ellipse) was computed according to the standard deviation of multiple suspended load measurements (Table 3). The total sediment yield exceeds the suspended load to account for the volume of material transported as bed load. A mean value of 20% of bedload would partly account for the systematic difference between predicted and measured denudation rate.

$\Delta H$ = 4 km. Given that landscape denudation is roughly at pace with fluvial incision, a value of $\Delta t_{response} \leq 1.6$ Myr would represent a maximum response time to tectonic forcing of the highest Himalayan peaks and thus for the whole landscape. Tectonic events older than early Pleistocene are thus not expected to have left a signature in present topography. The morphology of the HH and the river profiles are more probably still dynamically maintained by active tectonics.

**6.2.2. Present uplift profile in case of dynamic equilibrium.** In this section, we assume that present topography reflects present tectonics and that uplift pattern has been roughly constant during the Quaternary so that present topography and river profiles have reached an equilibrium. If the topography is approximately steady state, this equilibrium has to occur in a reference frame fixed relative to the MHT and thus attached to the Indian Plate, assuming that MHT geometry does not change during the Quaternary. In such a reference frame a steady state topography implies that rivers incise to compensate both rock uplift and the southward advance of the sloping bottom of the river channel due to advection of the hanging wall above the MHT:

$$v(x,t) = i(x,t) - S(x)c(t)\,, \qquad (16)$$

where $c(t)$ = 21 mm/yr is the shortening rate. In order to compare uplift rate profiles with those predicted by mechanical models of deformation, we have computed stacked rock uplift from the incision profiles according to (16) along the five rivers between the Sun Kosi and Kali Gandaki (Figure 12a).

**6.2.3. Present uplift profile and deformation at depth.** At least two different models of active deformation at depth have been proposed to explain present Himalayan topography (see section 2.2). Interseismic vertical deformation in central Nepal [*Jackson and Bilham*, 1994] roughly coincides with uplift profiles derived from fluvial incision in the HH (Figure 12a). As proposed by *Bilham et al.* [1997], part of this interseismic uplift might be unrecoverable and might contribute to building the High Range in the long term. According to this scheme, the front of the high range would have resulted from pervasive thrust faulting in the upper crust around the MCT. However, such a scenario appears improbable during the Holocene because as discussed by *Molnar* [1990], it would imply some shortening in addition to the 21 mm/yr absorbed at the MFT [*Lavé and Avouac*, 2000]. The total shortening rate across the range would then exceed the value obtained from GPS measurements [*Bilham et al.*, 1997]. In the western Himalayas, Holocene shortening rates across the Siwaliks belt [*Wesnousky et al.*, 1999] have been found to be similar to Quaternary rates [*Powers et al.*, 1998]. If such stability of the tectonic regime is confirmed in central Nepal, it would imply that pervasive thrust faulting in the upper crust around the MCT has been possibly limited since early Pleistocene.

Another solution would be that the front of the High Range and river knickpoints are maintained by overthrusting over the midcrustal ramp, inferred from the antiformal structure of the LH [*Schelling and Arita*, 1991]. Accordingly, the total shortening across the range would equal that accommodated by slip along the MFT, and the pattern of active uplift would be primarily controlled by the geometry of the MHT at depth. The pattern of uplift resulting from thrusting along the MHT associated with ductile flow in the lower crust has been computed from a mechanical model that also accounts for unloading/loading due to erosion/sedimentation [*Cattin and Avouac*, 2000]. Figure 12a shows the rock uplift rate predicted by this model for a 16° north dipping midcrustal ramp, which is consistent with the structural section in Figures 2 and 12c. This profile agrees fairly well with the uplift pattern, inferred from the incision profiles (Figure 12a). In the LH, modeled uplift rate is consistent with rock uplift <0.5 mm/yr at the latitude of the Katmandu basin. However, it does not account for ~1-2 mm/yr uplift rates around the Mahabarat because in this model, pervasive deformation localized at the MDT, MBT, or TKT, was neglected. Finally, it can be noted that in south Tibet the zone of uplift obtained from the model is broader than that derived from river incision.

The available data on active tectonics in the Himalayas and on fluvial incision are thus consistent with the simple view that surface deformation in the central Himalayas primarily reflects localized slip along the MHT at depth. Furthermore, uplift patterns derived from river incision provide some constrains on the MHT geometry. A planar MHT that dips uniformly at 8° from the MFT to beneath the HH (Figure 12b) would produce a significant rock uplift in the LH and in south Tibet [*Cattin and Avouac*, 2000], inconsistent with results from terrace study and river incision. The hypothesis of a deeply rooted MFT-MBT, as a modern tectonic equivalent of the MCT [*Mattauer*, 1975], would have led to similar inconsistencies.

## 7. Conclusions

Our study shows that in the Nepalese Himalayas, landscape denudation is roughly equal to fluvial incision. As observed in the Nanga Parbat region [*Burbank et al.*, 1996] and in New Zealand [*Hovius et al.*, 1997], we thus favor a model of landscape evolution in which bedrock landsliding, driven by river downcutting, is necessary to balance high rates of tectonic uplift (5 mm/yr) of the resistant crystalline rocks in the Higher Himalaya. Such a balance has probably prevailed over most of the Quaternary and still holds, as indicated by the comparison between denudation rates and sediment budgets over different time periods. These observations support the idea that the various feedback mechanisms between river incision, denudation of hillslopes, and crustal tectonics are probably very effective in reality.

From a methodological point of view our study shows that the analysis of the channel geometry of a modern river can be used to complement the record of river incision provided by fluvial terraces. This technique might be a useful means to investigate denudation in other active mountain belts where terraces are generally not preserved. However, the nonuniversality of such a simplified model (shear stress or stream power) in other geomorphologic settings [*Stock and Montgomery*, 1999; *Slingerland et al.*, 1998] suggests that comprehensive work on the physics of fluvial incision is still needed.

This study further illustrates how river incision profiles obtained from the geomorphic approach that we propose here may be used to assess tectonic models. The available data on active tectonics and denudation in the Himalayas of Nepal are shown to be consistent with the simple view that uplift in the Nepal Himalayas is primarily controlled by localized slip along the MHT with the topography being close to steady state. In our model the break in slope at the front of the HH is

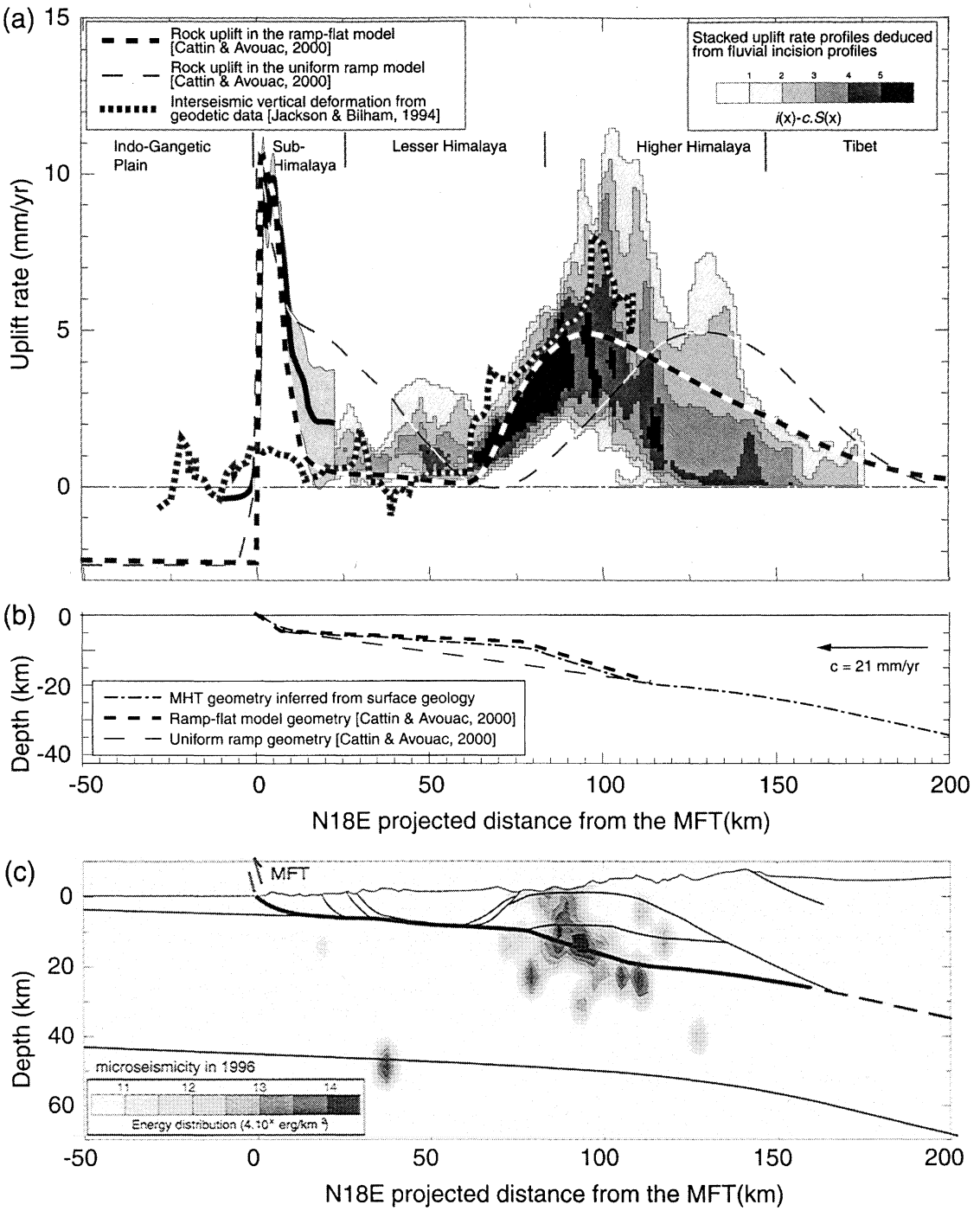


**Figure 12.** (a) Comparison between the stacked uplift rate profiles derived from fluvial incision rates with correction for horizontal advection (equation (16)) along the five trans-Himalayan rivers between Kali Gandaki and Sun Kosi and different models of tectonic uplift (dashed lines). Across the Siwaliks, the rock uplift profile along the Bagmati River [*Lavé and Avouac*, 2000] has been used. This long-term pattern of uplift was compared to interseismic vertical straining [*Jackson and Bilham*, 1994] and to the vertical deformation computed from a mechanical model [*Cattin and Avouac*, 2000]. This last profile results from thrusting along the MHT, ductile flow in the lower crust, and unloading/loading due to erosion/sedimentation. (b) Two different geometries tested for the MHT. Only the ramp-flat geometry accounts for fluvial incision pattern. (c) Correlation between the MHT geometry and the pattern of energy released by microseismic activity [*Pandey et al.*, 1995; *Lavé*, 1997].

simply the result of balanced erosion and tectonic uplift due to thrusting over a midcrustal ramp along the MHT. It is not necessary to invoke additional mechanisms as slip partitioning and thrust faulting near the front of the high range [*Bilham et al.*, 1997; *Seeber and Gornitz*, 1983] or late Miocene reactivation of the MCT [*Harrison et al.*, 1996]. We finally suggest that regressive erosion at the edge of the Tibetan Plateau [*Masek et al.*, 1994; *Montgomery*, 1994] cannot

account for present fluvial incision pattern. Although the role of glacial erosion is not discussed in this paper and would require further investigation, late Cenozoic enhanced erosion of the Himalayan front [*Molnar and England*, 1990; *Burbank*, 1992] is thus probably not the major factor in shaping the present Himalayan morphologic features. However, enhanced erosion may have helped by a feedback loop to focus deformation on a single range [*Beaumont et al.*, 1992] and to favor high vertical rock uplift in a narrow band and to prevent horizontal collapse [*Avouac and Burov*, 1996].

On the other hand, we note that 9 of the 14 highest peaks in the world are concentrated along a 500 km stretch that represents only a fifth of the total extent of the Himalayan arc. Their position north of the high uplifted area and not on its midpoint results directly from a strong asymmetry of the boundary conditions. On the northern side of the range the higher local base level and the rain shadow that induces a drop of fluvial shear stress both act to favor a position of the Nepalese/Tibetan drainage divide that is displaced to the north. However, the location of the high summits near the South Tibetan Detachment (STD) could also suggest a lithologic control on their position. According to a regional model of deformation the rate of shortening across the ranges decreases slightly westward [*Avouac and Tapponnier*, 1993; *Peltzer and Saucier*, 1996]. The structure and lithology of the range does not vary strongly laterally [e.g., *Gansser*, 1964]. The climatic conditions are more contrasted. Precipitation is maximal in the east and decreases gradually to the west. Variations in latitude along the arc probably do not induce important variations of the snowline or significant differences in the manner and amplitude glaciers curtail the growth of the Himalayan range [e.g., *Brozovic et al.*, 1997]. The location of the particularly elevated segment of the Higher Himalaya in the Nepalese central portion of the Himalayas does thus not seem to have any simple relation with any of those characteristics. It might therefore relate to the geometry of the MHT, characterized by a relatively steep midcrustal ramp in central Nepal, which would then be particularity limited to the central portion of the Himalayan arc.

## Appendix A: Fluvial Incision Profiles and Error Bar Computation

In order to estimate the uncertainties associated to the computation of shear stress and fluvial incision rate, we have adopted a conservative approach by considering the absolute error bar. Because we are primarily interested by the long-wavelength variations, we neglect spatial variations of variables at wavelength <10 km. We therefore deal with the uncertainties associated with estimates of slope, river width, pebble size, and discharge along smoothed profiles. The size of the sliding window is thus 10 km, and the profiles are oversampled every 1 km.

### A.1. River Slope Measurements

We use 1:63,000 topographic maps with elevation contour lines every 30 m. The average slope on a distance of 5 km can generally be measured with a good accuracy except in the Gangetic plain, where elevation contour lines are spaced by more than 5 km. Assuming an uncertainty on elevation of $\Delta H$ = 5 m for each contour level, the uncertainty on regional slope is $\Delta S/S = 2\Delta H/5000/S = 0.002/S$. In the deposition plain we assume $\Delta S/S \leq 30\%$.

### A.2. Width Measurements

The relative uncertainty on width measurement is of the order of 5% where the channel width exceeds the spatial resolution of the satellite or air photographs. Along the narrow reach there is a tendency for systematic overestimation of width measurement that depends on the pixel size $\Delta x$, by a factor $(1+1.5\Delta x/W)$ [*Lavé*, 1997]. In that case, we use an asymmetric error bar with a lower bound defined by $\Delta W_{inf}/W = 1.5\Delta x/W$. Where the absence of satellite image or aerial photographs preclude any width measurement, mainly for the most upstream reaches, we estimate the width according to the power law $W \propto Q^{0.5}$ [*Leopold*, 1994], and we assign an error bar of +200% / -50%.

### A.3. Discharge Estimation

We estimate the uncertainty to be of the order of $\Delta Q/Q$ = 25% uncertainty except in high range and southern Tibet, where the data are scarce. Moreover, our simple hydrodynamic model may not hold in that area because water discharge along the uppermost reaches also depends on water surge following snow melting. Conversely, our model probably overestimates runoff during precipitation on dry or unsaturated soils. We thus progressively raise the error bars northward up to $\Delta Q_{sup}/Q = 50\%$ and $\Delta Q_{inf}/Q = 100\%$.

### A.4. Pebble Size Estimation

We ascribe a symmetric error bar $\Delta D/D$ = 20% to encompass the observed variability of the pebble sizes measured along the Kali Gandaki [*Mezaki and Yabiku*, 1984]. In addition, we considered that by substituting Shields stress into the "classical" shear stress expression, we introduced a possible error in the incision law itself. The use of the shear stress would be equivalent to consider a constant mean gravel size $D$ = 5.5 cm along the whole river (mean value into the Kali Gandaki along its LH course). Accordingly, the revised error bar associated to the choice of the incision law will be

$\Delta D_{inf}/D = (D - 0.055)/D$ $\quad D > 0.055$,
$\Delta D_{sup}/D = (0.055 - D)/D$ $\quad D < 0.055$.

### A.5. Lithologic Calibration

The various units in the LH probably present important variation of erodability. However, by lack of information, we did not estimate any kind of error bar. Only a relative uncertainty of 20% is assumed for the HH gneisses, which traduces the error on the erodability ratio between Lesser and HH lithologies. A similar uncertainty was assumed for the Thetysian series.

**Acknowledgments.** We are most grateful to M.R. Pandey, R.P. Tandukar, and the National Seismological Center (DMG, Kathmandu) for the help in the organization of the field surveys, and to Steve Bergman for having kindly communicated to us his FT results on Everest. We are indebted to B. Hallet, who provided thoughtful reviews and comments. The manuscript benefited also from reviews and comments by an anonymous reviewer and from thorough comments by Pieter van der Beek. Part of this work has been done in PennState University (the postdoctoral support of the first author was received through Pennstate University and D. Burbank's NASA grant NAG5-7646) and at the Laboratoire de Géodynamique des Chaînes Alpines (LGCA).

## References


Anhert, F., Functional relationships between denudation, relief, and uplift in large mid-latitude drainage basins, *Am. J. Sci.*, *268*, 243-263, 1970.

Avouac, J. P., and E. Burov, Erosion as a driving mechanism of intracontinental mountain growth, *J. Geophys. Res.*, *101*, 17,747-17,769, 1996.

Avouac, J. P., and P. Tapponnier, Kinematic model of active deformation in central Asia, *Geophys. Res. Lett.*, *20*, 895-898, 1993.

Baade, J., A. Lang, R. Mäusbacher, and C. A. Wagner, Quaternary lake deposits in the Thakkhola Graben, Mustang, Nepal, in *13th Himalayas-Karakorum-Tibet International Workshop, Geol. Bull.*, *31*, pp. 22-23, Univ. of Peshawar, Pakistan, 1998.

Beaumont, C., P. Fullsack, and J. Hamilton, Erosional control of active compressional orogens, in *Thrust Tectonics*, edited by K.R. McClay, pp. 1-18, Chapman and Hall, New-York, 1992.

Bergman, S. C., D. Q Coffield, R. Donelick, J. Corrigan, J. Talbot, P. Cerveny and S. Kelley, Late Cenozoic compressional and extensional cooling and exhumation of the Qomolangma (Mt Everest) region, Nepal, *Geol. Soc. Am. Abstr. Programs*, *25*, 1993.

Bilham, R., K. Larson, J. Freymuller, and Project Idylhim Members, Indo-Asian convergence rates in the Nepal Himalayas, *Nature*, *386*, 61-64, 1997.

Brozovic, N., D. W. Burbank, and A. Meigs, Climatic limits on landscape development in the northwestern Himalaya, *Science*, *276*, 571-574, 1997.

Brunel, M., Ductile thrusting in the Himalayas: Shear sense criteria and stretching lineations, *Tectonics*, *5*, 247-265, 1986.

Brunsden, D., D. K. C. Jones, R. P. Martin, and J. C. Doornkamp, The geomorphological character of part of the Low Himalaya of eastern Nepal, *Z. Geomorph.*, *37*, 25-72, 1981.

Buffington, J. M., and D. R. Montgomery, A systematic analysis of eight decades of incipient motion studies, with special reference to gravel-bedded rivers, *Water Resour. Res.*, *33*, 1993-2029, 1997.

Bull, W., *Geomorphic Response to Climatic Change*, 326 pp., Oxford Univ. Press, New York, 1991.

Burbank, D. W., Causes of recent Himalayan uplift deduced from deposited patterns in the Ganges basin, *Nature*, *357*, 680-683, 1992.

Burbank, D. W., J. Leland, E. Fielding, R. S. Anderson, N. Brozovic, M. R. Reid, and C. Duncan, Bedrock incision, rock uplift and threshold hillslopes in the northwestern Himalayas, *Nature*, *379*, 505-510, 1996.

Carson, B., Erosion and sedimentation processes in the Nepal Himalayas, *Icimod Occasional Paper*, *1*, International Centre for Integrated Mountain Development (ICIMOD), Kathmandu, Nepal, 1985.

Cattin, R., and J. P. Avouac, Modelling mountain building and the seismic cycle in the Himalaya of Nepal, *J. Geophys. Res.*, *105*, 13,389-13,407, 2000.

Chang, H. H., *Fluvial Processes in River Engineering*, 425 pp., John Wiley, New York, 1988.

Delcaillau, B., *Les Siwaliks de l'Himalaya du Népal Oriental, Fonctionnement et Evolution*, 205 pp., CNRS, Paris, 1992.

Derry, L., and C. France Lanord, Himalayas weathering and erosion fluxes: Climate and tectonic controls, in *Tectonic Uplift and Climate Change*, edited by W.F. Ruddiman, pp. 289-312, Plenum, New York, 1997.

Duncan, C. C., A. J. Klein, J. G. Masek, and B. L. Isacks, Comparison of late Pleistocene and modern glacier extents in central Nepal based on digital elevation data and satellite imagery, *Quaternary Res.*, *43*, 241-254, 1998.

Fielding, E. J, B. L. Isacks, M. Barazangi, and C. C. Duncan, How flat is Tibet?, *Geology*, *22*, 163-167, 1994.

Foley, M. G., Quaternary diversion and incision, Deaborn river, Montana, Part I, *Geol. Soc. Am. Bull.*, *91*, 2152-2188, 1980a.

Foley, M. G., Bed-rock incision by streams, Part II, *Geol. Soc. Am. Bull.*, *91*, 2189-2213, 1980b.

Fort, M., Etude géomorphologique d'une chaîne de collision intracontinentale, mem. de thèse, 700 pp., Univ. de Paris VII, 1993.

Gansser, A., *Geology of the Himalayas*, Wiley Interscience, New York, 1964.

Gupta, V. J., On the stratigraphic position of the Kathmandu valley sediments, Nepal, *Geogr. Helv.*, *1*, 27-28, 1975.

Hancock, G. S., R. Anderson, and K. X. Whipple, Beyond power: Bedrock river incision process and form, in *Rivers over Rock: Fluvial Processes in Bedrock Channels*, *Geophys. Monogr. Ser.*, vol. 107, edited by K. J. Tinkler and E. E. Wohl, pp. 35-60, AGU, Washington, D. C., 1998.

Harrison, T. M., F. J. Ryerson, P. Le Fort, A. Yin, O. M. Lovera, and E. J. Catlos, A late Miocene-Pliocene origin for the central Himalayan inverted metamorphism, *Earth. Planet. Sci. Lett.*, *146*, E1-E7, 1997.

His Majesty's Government (HMG) of Nepal, Undertaking, Feasibility study on Sapt Gandaki hydroelectric power development project, report II, Nepal Electr. Auth., April 1982.

His Majesty's Government (HMG) of Nepal, Undertaking, Final report on disaster prevention master plan in upper Rapti river basin, Second Kulekhani Hydroelect. Proj., Nepal Electr. Auth., Oct. 1989.

His Majesty's Government (HMG) of Nepal, Bagmati command area development project, vol. 2, Minist. of Water Resour., Dept. of Irrigat., Dec. 1991a.

His Majesty's Government (HMG) of Nepal, Undertaking, Feasibility study - phase II, Nepal Electr. Auth., Upper Arun Hydroelect. Proj., Dec. 1991b.

His Majesty's Government (HMG) of Nepal, Undertaking, Middle Marsyandi hydroelectric Project, Nepal Electr. Auth., Eng. Dir. Invest. Dept., Aug. 1994.

His Majesty's Government (HMG) of Nepal, Climatological records of Nepal 1987-1990, Dept. of Hydrol. and Meteorol., Kathmandu, 1995a.

His Majesty's Government (HMG) of Nepal, Hydrological records of Nepal, Streamflow summary - 1993, 70 pp., Dept. of Hydrol. and Meteorol., Kathmandu, 1995b.

Hovius, N., Macroscale process systems of mountain belt erosion, in *Geomorphology and Global Tectonics*, edited by M.A. Summerfield, pp. 77-105, John Wiley, New York, 2000.

Hovius, N., C. P. Starck, and P.A. Allen, Sediment flux from a mountain belt derived by landslide mapping, *Geology*, *25*, 231-234, 1997.

Howard, A. D., Long profile development of bedrock channels: Interaction of weathering, mass wasting, bed erosion, and sediment transport, in *Rivers over Rock: Fluvial Processes in Bedrock Channels*, *Geophys. Monogr. Ser.*, vol. 107, edited by K. J. Tinkler and E. E. Wohl, pp. 297-319, AGU, Washington, D. C., 1998.

Howard, A. D., and G. Kerby, Channel changes in badlands, *Geol. Soc. Am. Bull.*, *94*, 739-752, 1983.

Howard, A. D., W. E. Dietrich, and M. A. Seidl, Modeling fluvial erosion on regional to continental scales, *J. Geophys. Res.*, *99*, 13,971-13,986, 1994.

Hurtrez, J. E., F. Lucazeau, J. Lavé, and J. P. Avouac, Investigation of the relationships between basin morphology, tectonic uplift and denudation from the study of an active fold belt in the Siwaliks Hills (central Nepal), *J. Geophys. Res.*, *104*, 12,779-12,796, 1999.

Ikeda, S., G. Parker, and Y. Kimura, Stable width and depth of straight grave rivers with heterogeneous bed material, *Water Resour. Res.*, *24*, 713-722, 1988.

Iwata, S., and T. Nakata, River terraces and crustal movement in the area around Narayanghat, Central Nepal, *J. Nepal Geol. Soc.*, *5*, 33-42, 1986.

Iwata, S., H. Yamanaka, and M. Yoshida, Glacial landforms and river terraces in the Thakkhola region, central Nepal, *J. Nepal Geol. Soc.*, *2*, 81-94, 1982.

Iwata, S., T. Sharma, and H. Yamanaka, A preliminary report on geomorphology of central Nepal and Himalayan uplift, *J. Nepal Geol. Soc.*, *4*, 141-149, 1984.

Jackson, M., and R. Bilham, Constraints on Himalayan deformation inferred from vertical velocity fields in Nepal and Tibet, *J. Geophys. Res.*, *99*, 13897-13912, 1994.

Jouanne, F., J. L. Mugnier, M. R. Pandey, J. F. Gamond, P. Le Fort, L. Serrurier, C. Vigny, and J. P. Avouac, Oblique convergence in the Himalayas of western Nepal deduced from preliminary results of GPS measurements, *Geophys. Res. Lett.*, *26*, 1933-1936, 1999.

Keller, E. A., Investigation of active tectonics: Use of surficial Earth processes, in *Active tectonics*, pp. 136-147, Nat. Acad. Press, Washington, D. C., 1986.

Koons, P. O., The topographic evolution of collisional mountain belts: A numerical look at the southern Alps, New Zealand, *Am. J. Sci.*, *289*, 1041-1069, 1989.

Krumbein, W. C., the effects of abrasion on the size, shape and roundness of rocks fragments, *J. Geol.*, *49*, 482-520, 1941.

Kuenen, P. H., Experimental abrasion of pebbles: 2. Rolling by current, *J. Geol.*, *64*, 336-368, 1956.

Kuhle, M., Der Dhaulagiri und Annapurna Himalaya. Ein Beitrag zur Geomorphologie extremer Hochgebirge, *Z. Geomorph., Suppl. 41 (2)*, 229 pp., 1982.

Laban, P., Field measurements on erosion and sedimentation in Nepal, Integrated Watershed Management Working, *Pap. 5*, Min. of For., Dep. of Soil and Water Conserv., Kathmandu, Nepal, 1978.

Larson, K., R. Bürgmann, R. Bilham, and J. T. Freymueller, Kinematics of the India-Eurasia collision zone from GPS measurements, *J. Geophys. Res.*, *104*, 1077-1093, 1999.

Lavé, J., Tectonique et érosion: L'apport de la dynamique fluviale a l'étude sismotectonique de l'Himalaya du Népal central, thèse de 3eme cycle, 225 pp., Univ. Paris VII, 1997.

Lavé, J., and J. P. Avouac, Active folding of fluvial terraces across the Siwaliks Hills (Himalayas of central Nepal), *J. Geophys. Res.*, *105*, 5735-5770, 2000.

Le Fort, P., Metamorphism and magmatism during the Himalayan collision, in *Collision Tectonics*, edited by M. P. Coward and A. C. Ries, *Geol. Soc. Spec. Publ.*, *19*, 159-172, 1986.

Leopold, L. B., *A View of the River*, 292 pp., Harward Univ. Press, Cambridge, Mass.,1994.

Leopold, L. B., and J.P. Miller, Ephemeral streams-hydraulics factors and their relation to the drainage net, *U.S. Geol. Surv. Prof. Pap.*, *282A*, 1-37, 1956.

Lyon-Caen, H., and P. Molnar, Constraints on the structure of the Himalayas from an analysis of gravity anomalies and flexural model of the lithosphere, *J. Geophys. Res.*, *88*, 8171-8191, 1983.

Lyon-Caen, H., and P. Molnar, Gravity anomalies, flexure of the Indian plate and the structure, support and evolution of the Himalayas and Ganga Basin, *Tectonics*, *4*, 513-538, 1985.

Masek, J.G., B. L. Isacks, M. Barazangi, and E. J. Fielding, Erosion and tectonics at the margins of continental plateaus, *J. Geophys. Res.*, *99*, 13,941-13,956, 1994.

Mattauer, M., Sur le mécanisme de formation de la schistosité dans l'Himalaya, *Earth Planet. Sci. Lett.*, *28*, 144-154, 1986.

Merritts, D. J., K. R. Vincent, and E. E. Wohl, Long river profiles, tectonism, and eustasy: A guide to interpreting fluvial terraces, *J. Geophys. Res.*, *99*, 14,031-14,050, 1994.

Métivier, F., and Y. Gaudemer, Stability of output fluxes of large rivers in south and east Asia during the last 2 million years. Implications on floodplain processes, *Basin Res.*, *11*, 293-303, 1999.

Métivier, F., Y. Gaudemer, P. Tapponnier, and M. Klein, Mass accumulation rates in Asia during the Cenozoic, *Geophys. J. Int.*, *137*, 280-318, 1999.

Mezaki, S., and M. Yabiku, Channel morphology of the Kali Gandaki and the Narayani rivers in central Nepal, *J. Nepal Geol. Soc.*, *4*, 161-176, 1984.

Molnar, P., Inversion of profiles of uplift rates for the geometry of dip-slip faults at depth, with examples from the Alps and the Himalayas, *Ann. Geophys.*, *5*, 663-670, 1987.

Molnar, P., A review of the seismicity and rates of active underthrusting and deformation at the Himalayas, *J. Himalayan Geol.*, *1*, 131-154, 1990.

Molnar, P., and P. England, Late Cenozoic uplift of mountain ranges and global climate change: Chicken or egg?, *Nature*, *346*, 29-34, 1990.

Montgomery, D. R., Valley incision and the uplift of mountain peaks, *J. Geophys. Res.*, *99*, 13,913-13,921, 1994.

Mugnier, J. L., P. Huyghe, E. Chalaron and G. Mascles, Recent movements along the Main Boundary Thrust of the Himalayas: Normal faulting in an over-critical thrust wedge?, *Tectonophysics*, *238*, 199-215, 1994.

Nakata, T., Geomorphic history and crustal movements of the foothills of the Himalayas, *Sci. Rep. Tohoku Univ. Ser. 2*, *22*, 177 pp., 1972.

Nakata, T., Active faults of the Himalayas of India and Nepal, *Spec. Pap. Geol. Soc. Am.*, *232*, 243-264, 1989.

Nautiyal, S.P., and P.N. Sharma, A geological report on the ground water investigation of Kathmandu valley, report, Geol. Surv. of India, 1961.

Pandey, M. R., R. P. Tandukar, J. P. Avouac, J. Lavé, and J. P. Massot, Interseismic strain accumulation on the Himalayan crustal ramp (Nepal), *Geophys. Res. Lett.*, *22*, 751-754, 1995.

Paola, C., and D. Mohrig, Paleohydraulics revisited: Paleoslope estimation in coarse-grained braided rivers, *Basin Res.*, *8*, 243-254, 1996.

Parker, G., Self-formed straight rivers with equilibrium banks and mobile bed, part 2, The gravel river, *J. Fluid Mech.*, *89*, 127-146, 1978.

Peltzer, G., and F. Saucier, Present-day kinematics of Asia derived from geologic fault rates, *J. Geophys. Res.*, *101*, 27,943-27,956, 1996.

Pinet, P., and M. Souriau, Continental erosion and large-scale relief, *Tectonics*, *7*, 563-582, 1988.

Powers, P. M., R. J. Lillie, and R. S. Yeats, Structure and shortening of the Kangra and Dehra Dun reentrants, Sub-Himalayas, India, *Geol. Soc. Am. Bull.*, *110*, 1010-1027, 1998.

Raymo, M. E, and W. F. Ruddiman, Tectonic forcing of the late Cenozoic climate, *Nature*, *359*,117-122, 1992.

Raymo, M. E., W. F. Ruddiman, and P. N. Froelich, Influence of late Cenozoic mountain building on ocean geochemical cycles, *Geology*, *16*, 649-653, 1988.

Schelling, D., The tectonostratigraphy and structure of the eastern Nepal Himalayas, *Tectonics*, *11*, 925-943, 1992.

Schelling, D., and K. Arita, Thrust tectonics, crustal shortening and the structure of the far-eastern Nepal Himalayas, *Tectonics*, *10*, 851-862, 1991.

Schmidt, K. M., and D. R. Montgomery, Limits to relief, *Science*, *270*, 617-620, 1995.

Searle, M.P., Extensional and compressional faults in the Everest-Lhotse massif, Khumbu Himalaya, *J. Geol. Soc. London*, *156*, 227-240, 1999.

Searle, M. P., R. R. Parrish, K. V. Hodges, A. Hurford, M. W. Ayres, and M. J. Whitehouse, Shisha Pangma leucogranite, south Tibetan Himalayas: Field relations, geochemistry, age, origin, and emplacement, *J. Geol.*, *105*, 295-317, 1997.

Seeber, L., and J. Armbuster, Great detachment earthquakes along the Himalayan arc and the long-term forecasts, in *Earthquake Prediction: An International Review, Maurice Ewing Ser.*, vol. 4, edited by D. W. Simpson and P. G. Richards, pp. 259-277, AGU, Washington, D. C., 1981.

Seeber, L., and V. Gornitz, River profiles along the Himalayan arc as indicators of active tectonics, *Tectonophysics*, *92*, 335-367, 1983.

Sheperd, R. G., and S. Schumm, Experimental study of river incision, *Geol. Soc. Am. Bull.*, *85*, 257-268, 1974.

Sklar, L., and W. E. Dietrich, River longitudinal profiles and bedrock incision modes: stream power and the influence of sediment supply, in *Rivers over Rock: Fluvial Processes in Bedrock Channels*, *Geophys. Monogr. Ser.*, vol. 107, edited by K. J. Tinkler and E. E. Wohl, pp. 237-260, AGU, Washington, D. C., 1998.

Slingerland, R., S. Willet, and N. Hovius, Slope-area scaling as a test of fluvial bedrock erosion laws, *EOS Trans. AGU*, *79* (45), Fall Meet. Suppl., F358, 1998.

Snyder, N. P., K. Whipple, G. E. Tucker, D. Merrits, Landscape response to tectonic forcing: DEM analysis of stream profiles in the Mendocino triple junction region, northern California, *Geol. Soc. Am. Bull.*, *112*, 1250-1263, 2000.

Stock, J. D., and D. R. Montgomery, Geologic constraints on bedrock river incision using the stream power law, *J. Geophys. Res.*, *104*, 4983-4993, 1999.

Stöcklin, J., Geology of Nepal and its regional frame, *J. Geol. Soc. London*, *137*, 1-34, 1980.

Stöcklin, J., Geological map of Kathmandu area and central Mahabarat range, sacle 1:250,000, Dep. of Mines and Geol., Népal, 1987.

Summerfield, M. A., and N. J. Hulton, Natural controls of fluvial denudation rates in major world drainage basins, *J. Geophys. Res.*, *99*, 13,871-13,883, 1994.

Wadia, D. N., The transitional passage of Pliocene into the Pleistocene in the Northwestern Sub-Himalaya, *Proc. 18th Int. Geol. Congr. London, 1948*, *10*, 43-48, 1951.

Weldon, R. J., Late Cenozoic geology of Cajon Pass: Implications for

tectonics and sedimentation along the San Andreas fault, Ph.D. thesis, 400 pp., Calif. Inst. of Technol., Pasadena, 1986.

Wesnousky, S. G., K. Senthil, R. Mohindra, and V. C. Thakur, Uplift and convergence along the Himalayan Frontal Thrust of India, *Tectonics*, *18*, 967-976, 1999.

West, R. M., and J. Munthe, Neogene vertebrate paleontology and stratigraphy of Nepal, *J. Nepal Geol. Soc.*, *1*, 1-14, 1981.

Whipple, K. X., E. Kirby, and S. H. Brocklehurst, Geomorphic limit to climate-induced increases in topographic relief, *Nature*, *401*, 39-43, 1999.

Willet, S, C. Beaumont, and P. Fullsack, Mechanical model for the tectonics of doubly vergent compressional orogens, *Geology*, *21*, 371-372, 1993.

Yamanaka, H., and S. Iwata, River terraces along the Middle Kali Gandaki and Marsyandi khola central Nepal, *J. Nepal Geol. Soc.*, *2*, 95-111, 1982.

Yanbin, W., and W. Jun, Fission-track evidence for episodic denudation of the Nyalam Higher Himalaya, China, in *13th Himalaya-Karakorum-Tibet International Workshop, Geol. Bull.*, *31*, p. 218, Univ. of Peshawar, Pakistan, 1998.

Yeats, R., and R. J. Lillie, Contemporary tectonics of the Himalayan frontal fault system: Folds, blind thrusts and the 1905 Kangra earthquake, *J. Struct. Geol.*, *13*, 215-225, 1991.

Yoshida, M., and Gautam, P., Magnetostratigraphy of Plio-Pleistocene lacustrine deposits in the Kathmandu valley, central Nepal, *Proc. Indian Nat. Sci. Acad.*, *54*A(3), 410-417, 1988.

Yoshida, M., and Y. Igarashi, Neogene to Quaternary lacustrine sediments in the Kathmandu valley, *J. Nepal Geol. Soc.*, *4*, 73-100, 1984.

Zhao, W., K. D. Nelson, and Project INDEPTH Team, Deep seismic reflection evidence for continental underthrusting beneath southern Tibet, *Nature*, *366*, 55-559, 1993.

Zollinger, F., The Sapt Kosi unsolved problems of flood control in the Nepalese Terai, integrated watershed management, torrent control and use development of soil and water conservation, Dept. of Soil and Water Conserv., Kathmandu, Nepal, 1979.

J. P. Avouac, Laboratoire de Géophysique, CEA, F-91680, Bruyères-Le-Châtel, France. (avouac@ldg.bruyeres.cea.fr)

J. Lavé, Laboratoire de Géodynamique des Chaînes Alpines, BP 53, F-38041 Grenoble, France. (jlave@ujf-grenoble.fr)

(Received February 28, 2000; revised May 13, 2001;
Accepted June 9, 2001.)